



HAL
open science

Modelling nuclear fuel behaviour with TAF-ID: Calculations on the VERDON-1 experiment, representative of a nuclear severe accident

E. Geiger, C. Guéneau, Y. Pontillon, E.C. Corcoran

► To cite this version:

E. Geiger, C. Guéneau, Y. Pontillon, E.C. Corcoran. Modelling nuclear fuel behaviour with TAF-ID: Calculations on the VERDON-1 experiment, representative of a nuclear severe accident. *Journal of Nuclear Materials*, 2019, 522, pp.294 - 310. 10.1016/j.jnucmat.2019.05.027 . hal-03487013

HAL Id: hal-03487013

<https://hal.science/hal-03487013>

Submitted on 20 Dec 2021

HAL is a multi-disciplinary open access archive for the deposit and dissemination of scientific research documents, whether they are published or not. The documents may come from teaching and research institutions in France or abroad, or from public or private research centers.

L'archive ouverte pluridisciplinaire **HAL**, est destinée au dépôt et à la diffusion de documents scientifiques de niveau recherche, publiés ou non, émanant des établissements d'enseignement et de recherche français ou étrangers, des laboratoires publics ou privés.



Distributed under a Creative Commons Attribution - NonCommercial 4.0 International License

Modelling nuclear fuel behaviour with TAF-ID: Calculations on the VERDON-1 experiment, representative of a nuclear severe accident

E. Geiger^{1,2}, C. Guéneau², Y. Pontillon³, E. C. Corcoran¹

¹Department of Chemistry and Chemical Engineering, Royal Military College of Canada, PO Box 17000, Station Forces, Kingston, Ontario K7K 7B4, Canada

²Commissariat à l'Énergie Atomique et aux Énergies Alternatives, Centre de Saclay, DEN-DPC-SCCME, 91191 Gif-sur-Yvette, France

³Commissariat à l'Énergie Atomique et aux Énergies Alternatives, Centre de Cadarache, DEN-DEC-SA3E F-13108 Saint-Paul-lez-Durance, France

Keywords: Nuclear Severe Accident, Thermodynamic modelling of nuclear fuel, TAF-ID, VERDON

Abstract:

The chemical behaviour of the main elements present in a PWR irradiated fuel sample (UO₂ fuel, Zr from the Zircaloy-cladding, Pu, Np, and fission products such as Ba, Ce, Cs, Gd, I, La, Mo, Nd, Pd, Rh, Ru, Sr, Tc, Te, etc.) submitted to a nuclear severe accident type sequence (VERDON-1 experiment) has been investigated by thermodynamic calculations using the TAF-ID database. Particular emphasis has been placed on the chemical behaviour of the fission products Ba, Cs, Mo, and Zr, and the interactions between the Zircaloy-cladding and the UO₂ matrix. Calculation results have been compared to experimental observations completed during the VERDON-1 experiment (instantaneous release of fission products and final chemical state of elements in the sample). Results presented in this manuscript do not account for non-equilibrium phenomena that have a major impact on fission product behaviour (e.g., chemical diffusion, mass transport induced by temperature gradients in the fuel pellet, etc.). None the less, these TAF-ID calculations have described accurately the melting of the sample following the formation of a mixed (U,Zr)O_{2-x} phase because of the interaction between the fuel and the Zircaloy-cladding. Furthermore, calculations have assisted in the explanation of the instantaneous released fractions observed for Ba and Mo during the experiment (as a function of the experiment atmosphere and temperature).

1. INTRODUCTION

The accurate prediction of the phase equilibria and thermodynamic properties of nuclear fuels during the nuclear fuel cycle is of utmost importance to the understanding of high temperature physicochemical behaviour for the purposes of quality specifications, process optimization, safety improvements, etc. Furthermore, predicting the behaviour at high temperature of the UO₂ fuel containing fission products and its interaction with the Zircaloy-cladding and other structural materials and nuclear reactor components (e.g., neutron absorbers, alloys, concrete, etc.) is mandatory for estimating the progression of severe accidents, their consequences, and establishing mitigation measures. For all this, a comprehensive, internationally recognized, and quality-assured nuclear materials thermodynamic database is required. The Thermodynamic of Advanced Fuels – International Database (TAF-ID) project [1,2] answers this need by developing a thermodynamic database using the CALPHAD method [3] for the design of Generation 4 reactors and for lifetime extension, safety improvement, and safety analysis for Generation 2 & 3 reactors. The project is a collaboration between 10 organisations from seven countries (i.e., CEA, CNL, CRIEPI, TU Delft, JAEA, KAERI, NNL, DoE, Ontario Tech University, and RMC) coordinated by the Organisation for Economic Co-operation and Development (OECD)-Nuclear Energy Agency (NEA). Thermodynamic calculations on different types of fuel (e.g., mainly oxide and metallic) including minor actinides (e.g., Am,

Np), fission products (*e.g.*, Cs, I, Ba, Sr, Mo, Zr, lanthanides, metallic fission products) can be performed with this database. Also, structural materials such as steel, fuel cladding, concrete, and absorber alloys (B₄C and AlC) can be considered for high temperature chemical interactions calculations.

At this advanced degree of development, it was necessary to validate the current database by comparison to experimental data on complex systems. The VERDON-1 experiment [4,5] was an excellent case study as it reproduced a nuclear severe accident at laboratory scale and extensive characterisation was performed during and after the experiment [5–8]. Particularly, the VERDON programme objectives were to:

- Acquire data on fission products release from PWR irradiated fuels (both UO₂ and (U,Pu)O₂ fuels) during a nuclear severe accident, as a function of temperature and under different atmospheres (consisting of varying ratios of steam/hydrogen).
- Determine the chemical interactions between the phases formed during irradiation (caused by the formation of fission products), the fuel matrix (UO₂, (U,Pu)O₂), and the Zircaloy-cladding, that may take place during a nuclear severe accident.

Nevertheless, the TAF-ID is a thermodynamic database and therefore it does not account for the non-equilibrium phenomena that take place during irradiation (many of which are summarized in [9]) and during a severe accident. For instance, kinetic phenomena (*e.g.*, athermal radiation-enhanced diffusion of the elements and thermal diffusion under temperature gradient), irradiation effects (*e.g.*, defect generation and propagation, *etc.*), and other thermomechanical phenomena (*e.g.*, swelling, fuel pores interconnection at high temperature, *etc.*), are not considered in thermodynamic calculations with the TAF-ID. To account for these phenomena, the database should be coupled using a Gibbs energy minimizer software to specific software or integral multi-physics codes (fuel performance codes and/or severe accident codes) to simulate the nuclear fuel behaviour at both normal and off-normal conditions [10–15]. Also, the heterogeneous distribution of some fission products in the fuel section is not taken into account. Knowing these limitations, the objective of this manuscript is to evaluate the capabilities of thermodynamic calculations with the TAF-ID database and its performance for the calculation of irradiated nuclear fuel chemical behaviour in real scenarios, by taking the VERDON-1 experiment as a reference.

The main details of the VERDON-1 experiment are recalled in section 2. Section 3 reviews the input data used for TAF-ID calculations. Section 4 presents the calculation results (*i.e.*, the chemical phase compositions and their evolution during the VERDON-1 experiment) and focuses on the fission products Ba, Cs, I, and Mo, and the Zircaloy-cladding and fuel interactions. Finally, section 5 compares the released fractions determined experimentally and VERDON-1 sample post-mortem characterisation results [5–7] to the TAF-ID calculation results from this work.

2. VERDON-1 EXPERIMENT MAIN CHARACTERISTICS

2.1. SAMPLE DESCRIPTION

The VERDON-1 sample characteristics are described in [5,6,8] so only the main points are recalled below in **Figure 1** and **Table 1**. The VERDON-1 sample consisted of two irradiated UO₂ pellets with two un-irradiated half pellets of depleted UO₂ at each side, in the original M5 cladding (referred to as Zircaloy-cladding in this manuscript). The father rod, from which the two irradiated pellets were taken, was irradiated up to 72 GWd.t⁻¹ in the Gravelines-5 reactor. The VERDON-1 sample was re-irradiated in

the OSIRIS materials testing reactor at 10 W.cm^{-1} to re-create the short-lived isotopes (e.g., ^{99}Mo , ^{132}Te , ^{133}I , ^{131}I , ^{140}Ba , etc.).

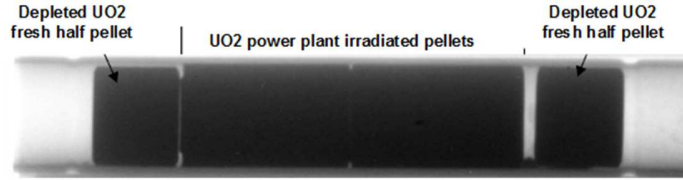


Figure 1: VERDON-1 sample

Table 1: VERDON-1 sample characteristics

Cladding	M5	Pellet mean diameter (mm)	8
Ext. Diameter (mm)	9.5	Pellet mean height (mm)	14
Fuel type	UO ₂	Density (% TD)	95.31

Extensive characterisation results on the initial state of the sample microstructure and the different elements are available in Ref. [8]. The main observations were: (1) high burn-up region extending up to $60 \mu\text{m}$ from the periphery towards the centre of the fuel, (2) existence of an internal ZrO_2 layer (15 to $20 \mu\text{m}$ from the periphery of the sample), and (3) most of the inventory of fission products and other elements produced by irradiation (e.g., Pu) were located in the peripheral region of the sample. Mo-Ru metallic precipitates were clearly observed, and also Cs-O precipitates, though their exact chemical composition could not be determined. No particular association nor precipitates of other elements were observed in the sample. Therefore, the initial chemical state of the elements is not completely known, and it is presumably not in thermodynamic equilibrium for the reasons listed in [9].

2.2. THERMAL-HYDRAULIC SEQUENCE

The thermal-hydraulic sequence of the VERDON-1 experiment is described in [5,8]. The sequence consisted of four stages, each with different temperatures and atmospheres in contact with the sample. The conditions of each stage are presented in **Table 2**, along with the calculated oxygen potential values for stages 2 and 3.

The first stage of the experiment consisted of a temperature ramp from room temperature up to $400 \text{ }^\circ\text{C}$ under a flow of helium. The oxygen potential of the system during this stage was fixed by the fuel, Zircaloy-cladding, and fission products interactions. The second stage consisted of a temperature ramp under an oxidizing mix of steam-hydrogen from 400 to $1500 \text{ }^\circ\text{C}$ with a temperature plateau at $1500 \text{ }^\circ\text{C}$ (to ensure the oxidation of the Zircaloy-cladding). The third stage consisted of a temperature ramp from 1500 to $2400 \text{ }^\circ\text{C}$ under a reducing mix of steam-hydrogen with temperature plateaus every $100 \text{ }^\circ\text{C}$. Lastly, the fourth stage of the experiment consisted of a temperature ramp from 2400 to $2611 \text{ }^\circ\text{C}$ under a flow of helium. During the fourth stage fuel melting and relocation was initiated and the oxygen potential of the system was fixed by the UO₂ fuel, Zircaloy-cladding, and fission products interactions.

Table 2: VERDON-1 atmosphere characteristics [8]

	Temperature	Atmosphere	Oxygen Potential
Stage 1	Ambient to 400 °C Plateau at 400 °C for 1 h.	Neutral Carrier: He	Fixed by the sample
Stage 2	400 °C to 1500 °C 1 h plateau at 1500 °C	Oxidizing H ₂ O = 25 mg.s ⁻¹ H ₂ = 0.45 mg.s ⁻¹ Carrier: He	From -400 kJ.mol ⁻¹ (400 °C) to -244 kJ.mol ⁻¹ (1500 °C)
Stage 3	1500 °C to 2400 °C	Reducing H ₂ O = 0.3 mg.s ⁻¹ H ₂ = 0.33 mg.s ⁻¹ Carrier: He	From -365 kJ.mol ⁻¹ (1500 °C) to -279 kJ.mol ⁻¹ (2611 °C)
Stage 4	2400 °C to 2611 °C	Neutral Carrier: He	Fixed by the sample

2.3. CHARACTERISATIONS DURING AND AFTER THE EXPERIMENT

As described in Ref. [5], two gamma-ray spectrometry stations measured the fuel sample activity during the experiment, allowing for the instantaneous release measurement of different isotopes as a function of time, temperature, and atmosphere. Also, by gamma-ray monitoring, the presence of non-volatile species (*e.g.*, ⁹⁵Zr and ¹⁴⁰La) allowed for time determination (and thereby the temperature) at which the fuel would melt and collapse (*i.e.*, a sudden decrease in the measured signal of these elements implies the melting and relocation of the sample).

After the experiment, Electron Probe Micro Analysis (EPMA) and Scanning Electron Microscopy (SEM) were performed, as described in [6]. These characterisations allowed determining the chemical composition of the phases present after the experiment, the sample microstructure, and interactions with the Zircaloy-cladding. In this work, TAF-ID calculation results (from input parameters that mimic the condition parameters used in the VERDON-1 experiment) are compared to the experimental observations completed during and after the VERDON-1 experiment.

3. DATA INPUT PARAMETERS FOR TAF-ID CALCULATIONS

It must be noted that the partners responsible of the VERDON program have not made public the exact elemental composition of the sample. Therefore, the initial element concentrations are the result of CESAR III [16] calculations for a similar fuel as the one used in VERDON-1, except that the considered fuel had an initial Pu content equal to 4.5 wt% and the fuel burn-up was 60 GWd.t⁻¹. The concentrations calculated with CESAR III were lineally extrapolated to account for the extra burn-up. Fifteen elements have been considered for the calculation, for which concentrations have been estimated considering the CESAR III ratios per mole of uranium and the mass and density of the irradiated pellets. The UO₂ contribution from the un-irradiated half pellets has also been considered in the overall composition. The Zr amount corresponding to the Zircaloy-cladding was calculated considering its longitude, internal and external diameters, pure metallic Zr density, and Zr molar mass. After each stage, only the moles of each element

that remain in a condensed phase have been considered for calculating the following stage, as the balance is considered to have been “*released*” from the sample into the gaseous phase. As for the atmosphere, the hydrogen and steam flows for each stage have been multiplied by the duration of the corresponding stage. During stage 1 of the experiment, only helium flowed over the sample and therefore the oxygen chemical potential of the system depended strongly on the deviation from stoichiometry in the UO_2 ($\text{UO}_{2\pm x}$). As a very small deviation from stoichiometry would have a major impact on the fission products chemical state and no experimental data were available regarding the stoichiometry of the UO_2 fluorite phase after irradiation, no TAF-ID calculations have been performed for stage 1.

In the TAF-ID calculations for stages 2, 3, and 4, thermodynamic equilibrium between the gas and the condensed phases is assumed. Also, calculations for these stages assume that all the elements are homogeneously mixed in the system (fuel, Zircaloy-cladding, and fission products), which in the real system is not the case. This assumption gives the direction towards which the system will tend to evolve. The irradiated nuclear fuel in normal conditions (initial state) is not at thermodynamic equilibrium, and some fission products phases predicted by thermodynamics calculations are not observed in irradiated fuels. Moreover, the chemical state of some fission products is still not well known. Nevertheless, at higher temperatures, above 1600 °C, the diffusion rate of the metallic elements is expected to be sufficiently high for the phases to form, even if the reactions may not be complete. This point will be further discussed in this paper.

The resulting input data for each stage during the VERDON-1 experiment are presented in **Table 3**. Calculations are performed using the Thermo-Calc software [17] and TAF-ID version 8 (January 2018 version).

Table 3: Data input conditions for VERDON-1 calculations

Stage 2		Stage 3		Stage 4	
Duration (s)	16522	Duration (s)	6842	Duration (s)	1362
Atmosphere		Atmosphere		Atmosphere	
H ₂ (g)	7.435	H ₂ (g)	2.258	He (g)	8.172
H ₂ O (g)	413.050	H ₂ O (g)	2.053		
System composition		System composition		System composition	
Element	moles	Element	moles	Element	moles
Ba	1.5338E-04	Ba	1.4777E-04	Ba	6.1139E-06
Ce	2.4874E-04	Ce	2.4875E-04	Ce	2.4767E-04
Cs	2.9101E-04	Cs	0	Cs	0
Gd	1.3570E-05	Gd	1.3570E-05	Gd	1.3599E-05
I	2.3318E-05	I	0	I	0
La	1.1969E-04	La	1.1969E-04	La	8.4386E-05
Mo	4.7928E-04	Mo	9.6123E-05	Mo	8.2088E-05
Nd	3.7132E-04	Nd	3.7133E-04	Nd	3.7099E-04
Np	2.3806E-05	Np	2.3806E-05	Np	2.3628E-05
O (Fuel)	1.6410E-01	O	2.6186E-01	O	2.5809E-01
Pd	1.9225E-04	Pd	1.1000E-04	Pd	0
Pu	3.5526E-04	Pu	3.5501E-04	Pu	3.5490E-04
Rh	5.4488E-05	Rh	5.4475E-05	Rh	2.5560E-05
Ru	3.3198E-04	Ru	3.3196E-04	Ru	3.1519E-04
Sr	1.2958E-04	Sr	1.2956E-04	Sr	1.2479E-04
Tc	1.1000E-04	Tc	1.1000E-04	Tc	1.1000E-04
Te	5.2480E-05	Te	0	Te	0
U	5.2492E-02	U	5.2480E-02	U	5.1715E-02
Zr (Cladding)	7.6354E-02	Zr	7.6881E-02	Zr	7.6899E-02
Zr (FP)	5.2822E-04				

4. CALCULATION RESULTS

4.1. OXYGEN CHEMICAL POTENTIAL EVOLUTION

The evolution of the oxygen chemical potential of the system, defined as $\mu_{O_2} = R \cdot T \cdot \ln(P_{O_2})$, during stages 2, 3, and 4 is presented in **Figure 2**. According to calculations, at the beginning of stage 2 the oxygen chemical potential is $-400.5 \text{ kJ}\cdot\text{mol}^{-1}$ and it increases up to $-245.1 \text{ kJ}\cdot\text{mol}^{-1}$. When the atmosphere is switched to reducing, the oxygen potential of the system drops to $-364.8 \text{ kJ}\cdot\text{mol}^{-1}$ but it increases up to $-293.8 \text{ kJ}\cdot\text{mol}^{-1}$ at the end of stage 3. The linear behaviour of the oxygen potential during stages 2 and 3 indicates that it is imposed by the water equilibrium in the atmosphere. On the other hand, only helium flows in the circuit during stage 4 and the oxygen potential is only influenced by the chemical equilibria of the sample. It is observed that, at the beginning of this stage, the oxygen potential is practically constant and equal to $-340.8 \text{ kJ}\cdot\text{mol}^{-1}$. As it will be developed below, the sharp decrease observed on the oxygen

potential at 2504 °C (from -304.1 to -392.0 kJ.mol⁻¹) is associated to a solid-liquid transition of the solid solution formed by the interaction between the oxidized Zircaloy-cladding and the fuel.

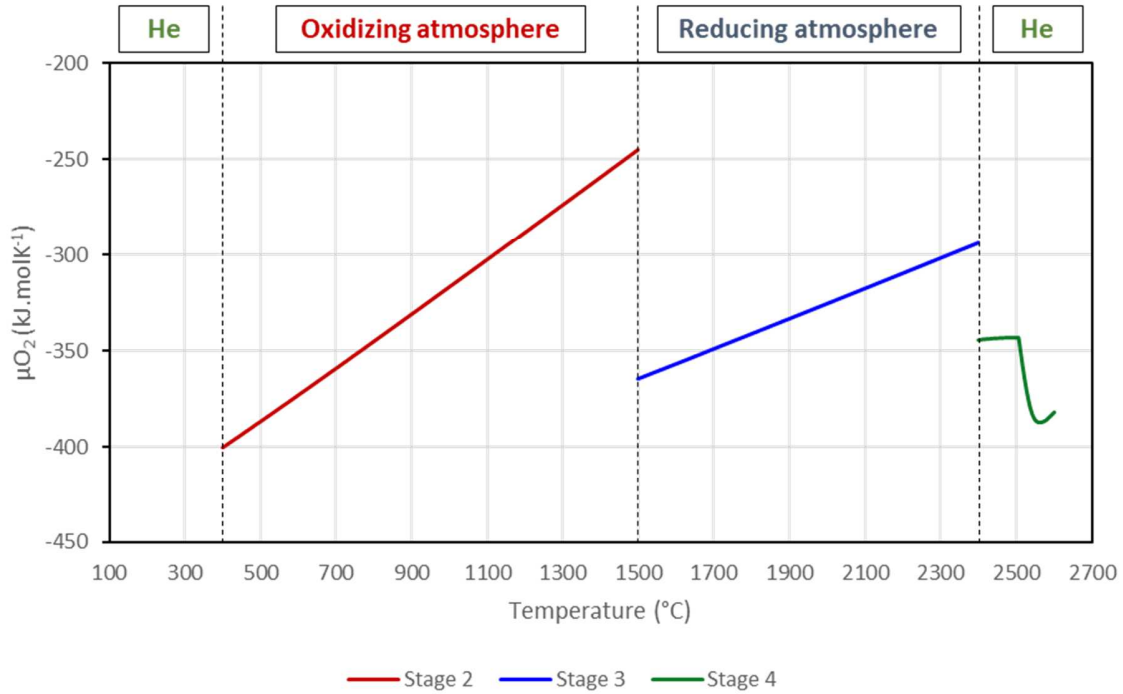


Figure 2: Oxygen chemical potential evolution during stages 2, 3, and 4

4.2. ELEMENTS DISTRIBUTION BETWEEN THE GASEOUS AND CONDENSED PHASES

Assuming thermodynamic equilibrium between the condensed phases (solid and liquid) and the gas phase, the elemental gas fractions as well as the evolution of the condensed phase fractions are calculated with the TAF-ID for every element listed in **Table 3**, as a function of both temperature and oxygen potential. Only results regarding five representative elements (*i.e.*, Ba, Cs, I, Mo, and Zr) are described in the text below. These elements have a particular impact on the chemistry of other fission products (particularly Mo [18]) and are representative of the volatile (Cs), semi-volatile (Ba and Mo, both of which have chemical behaviours that depend strongly on the oxygen potential), and low-volatile (Zr) categories of fission products [19]. First, the calculated Zr behaviour is presented since its high concentration in the system (due to the consideration of the Zircaloy-cladding) has an important impact on the other elements and on the oxygen potential of the system. Secondly, Cs and I calculated behaviour is presented, followed by that of Ba, and then Mo. Lastly, the evolution of all the chemical phases and a summary of the calculated interactions are presented. Results presented in this section are compared to experimental observations in section 5.

Zirconium

The calculated Zr evolution for stages 2, 3, and 4 is presented in **Figure 3**. For stage 2, under oxidizing atmosphere, these calculations indicate that:

- Zr is found in an oxidized state as monoclinic ZrO₂ (ZrO₂-M) from the beginning of the experiment. Traces of Zr are also dissolved in the fluorite phase (UO₂). Though the dissolved quantity of

zirconium in the UO_2 is still negligible at low temperature, it increases up to $1.7 \cdot 10^{-3}$ moles (2.5% of the Zr present in the system) at the end of stage 2.

- At 1105 °C there is a phase transition in the ZrO_2 , from monoclinic ($\text{ZrO}_2\text{-M}$) to tetragonal ($\text{ZrO}_2\text{-T}$). Both uranium and barium are soluble in the latter phase. At the end of stage 2, 97.8% of Zr is found as tetragonal $(\text{Zr}_{0.97}\text{U}_{0.03})\text{O}_2\text{-T}$ and 2.2% is dissolved in the $(\text{U}_{0.991}\text{Zr}_{0.009})\text{O}_{2.003}$ fluorite phase.

Regarding stage 3, when the atmosphere becomes reducing, calculations indicate that:

- Despite the oxygen chemical potential (μ_{O_2}) change from -245.1 to -364.8 $\text{kJ}\cdot\text{mol}^{-1}$ at the beginning of the stage, the chemical state of Zr is quite similar to that at the end of stage 2. Indeed, 97.6% of Zr is in the $(\text{Zr}_{0.97}\text{U}_{0.03})\text{O}_2\text{-T}$ phase and 2.4% is dissolved in the $(\text{U}_{0.991}\text{Zr}_{0.009})\text{O}_{1.9995}$ fluorite phase.
- The Zr fraction dissolved in the fluorite increases up to 5.9% ($(\text{U}_{0.975}\text{Zr}_{0.025})\text{O}_{1.997}$) at 1675 °C, but at these conditions a miscibility gap appears and a second fluorite phase is formed: $(\text{U}_{0.835}\text{Zr}_{0.165})\text{O}_{1.986}$.
- At 1788 °C, BaZrO_3 (perovskite structure) is formed, better observed in the Ba behaviour section (below).
- By 1947 °C, 99.7% of Zr in the system is present in the $(\text{U}_{0.71}\text{Zr}_{0.29})\text{O}_{1.993}$ fluorite phase and 0.3% is under BaZrO_3 form.
- At 2108 °C, BaZrO_3 becomes unstable and all the Zr in the system is in the $(\text{U}_{0.7}\text{Zr}_{0.3})\text{O}_{1.992}$ fluorite phase until the end of stage 3.

Thus during stage 3 the mixed oxide $(\text{U,Zr})\text{O}_2$ is reduced into a $(\text{U,Zr})\text{O}_{2-x}$ phase, which is able to incorporate increasing amounts of zirconium as the temperature increases.

During stage 4, when the steam and hydrogen flows are stopped and only helium flows through the system, calculations indicate that:

- Starting at 2505 °C, the $(\text{U,Zr})\text{O}_2$ phase undergoes a solid-liquid transition and Liquid A is formed. The mixed oxide is fully molten at 2578 °C and retains the fission products (Ce, Nd, La, etc.) that were dissolved in the solid phase. This solid-liquid transition decreases the oxygen chemical potential of the system from -341 to -392 $\text{kJ}\cdot\text{mol}^{-1}$ which, as observed below, has an important impact on the behaviour of the other elements.
- At the end of stage 4, 99.7% of Zr remains in the liquid phase and 0.3% is present in the gaseous phase as $\text{ZrO}_{(\text{g})}$ and $\text{ZrO}_{2(\text{g})}$ species.

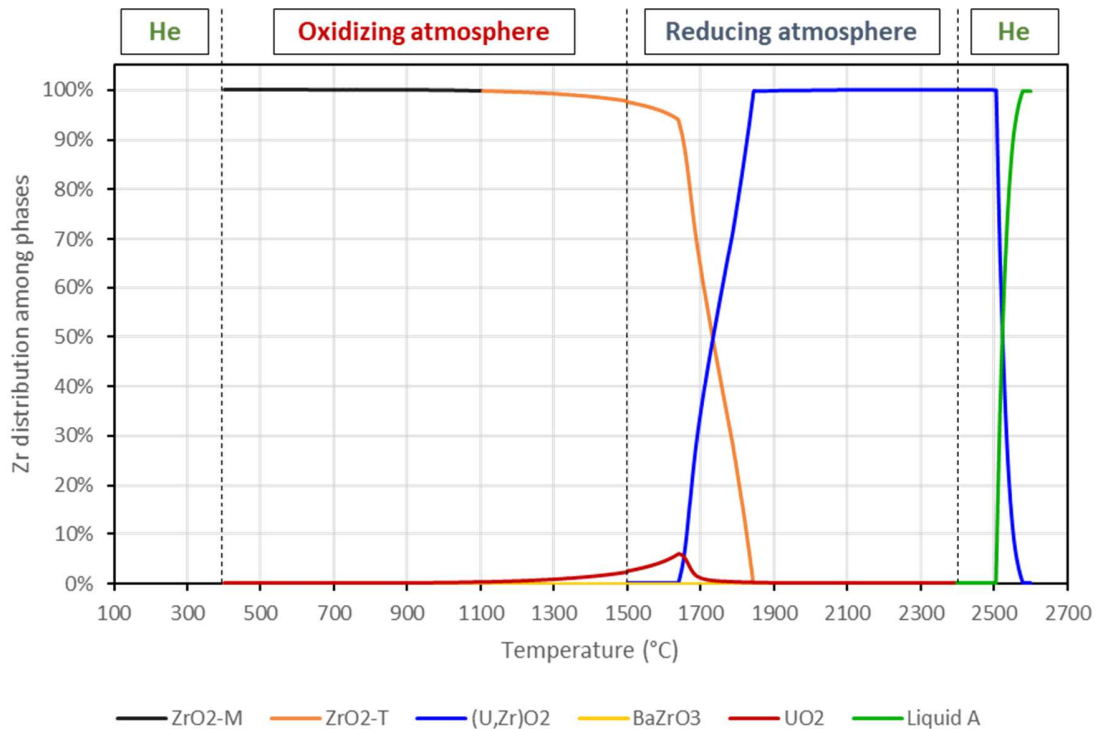


Figure 3: Calculated chemical evolution of zirconium during the VERDON-1 experiment

Caesium and iodine

The calculated Cs and I chemical evolution is presented in **Figure 4**. According to these calculations:

- At the beginning of stage 2, caesium exists mainly as Cs_2MoO_4 in an orthorhombic structure ($\text{Cs}_2\text{MoO}_4\text{-O}$, 92% of the total Cs) and as CsI (8%, which represents 100% of the iodine in the system).
- CsI volatilizes by 465 °C and remains in the gaseous phase for the rest of the experiment.
- At 579 °C a phase transition takes place in the Cs_2MoO_4 phase, from orthorhombic to hexagonal ($\text{Cs}_2\text{MoO}_4\text{-H}$), without any impact on the elements distribution.
- Above 652 °C $\text{Cs}_2\text{MoO}_4\text{-H}$ evaporates progressively (with Cs present in the gas phase mainly as Cs_2MoO_4).
- At 776 °C the remaining $\text{Cs}_2\text{MoO}_4\text{-H}$ becomes liquid, forming Liquid B. The composition and evolution of this liquid is presented in **Figure 5**. As observed, this phase is mainly composed of O, Cs, Mo, and Ba.
- At 974 °C all Cs is in the gas phase, mainly as Cs_2MoO_4 and CsI.
- Liquid B appears once more at 1135 °C because of the solid-liquid transition of BaMoO_4 , which dissolves a fraction of the Cs in the gaseous phase.
- At the end of stage 2 all Cs and I are in the gaseous phase, therefore these elements were not considered for further calculations on stages 3 and 4.

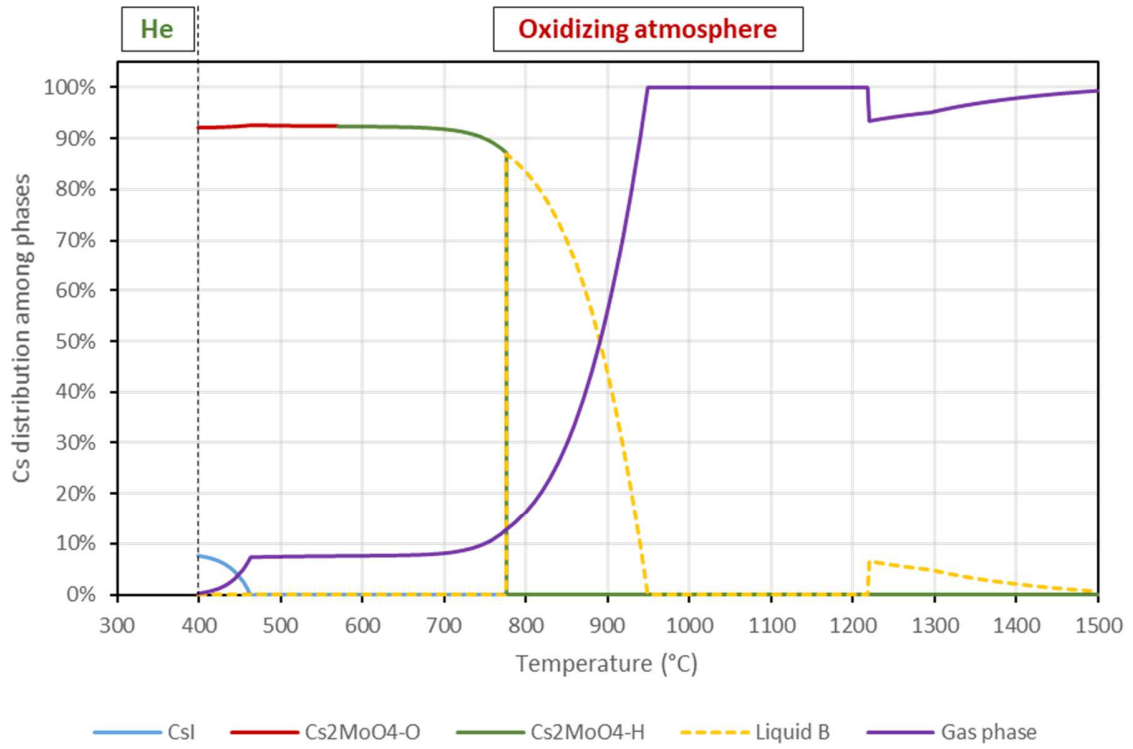


Figure 4: Calculated chemical evolution of caesium and iodine during the VERDON-1 experiment

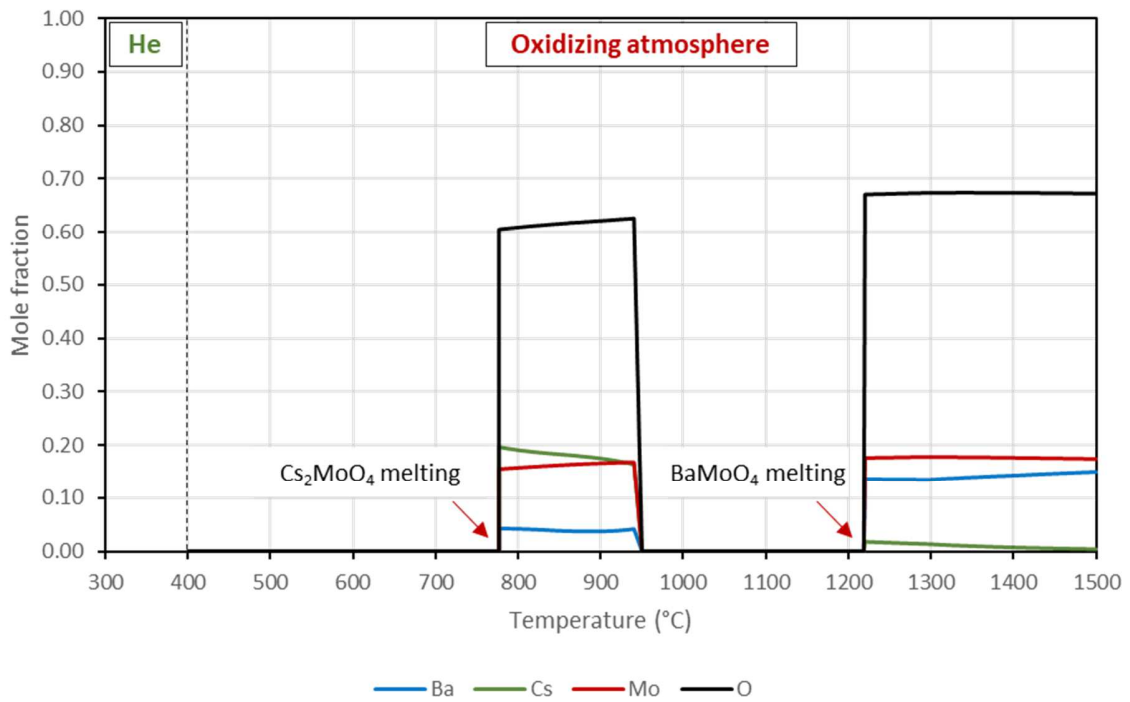


Figure 5: Evolution of Liquid B composition during stage 2

Barium

The calculated Ba distribution among the different phases for stages 2, 3, and 4 is presented in **Figure 6**. For stage 2, these calculations indicate that:

- Ba exists exclusively as BaMoO₄ at the beginning of the stage.
- At 776 °C, Liquid B is formed because of the solid-liquid transition of Cs₂MoO₄-H, which dissolves up to 35.3% of the total barium in the system. Once this liquid phase disappears at 950 °C (because of the complete volatilisation of Cs) Ba returns to the BaMoO₄ phase.
- At 1105 °C, following the phase transition in the ZrO₂ phase from monoclinic to tetragonal, a fraction of Ba is dissolved. As temperature increases, Ba dissolved fraction in the ZrO₂-T phase increases as the initial BaMoO₄ is decomposed.
- The solid-liquid transition of the remaining BaMoO₄ takes place at 1220 °C and Liquid B is formed once again. The total amount of this liquid phase decreases as temperature increases, mainly because of the dissolution of Ba into the ZrO₂-T and the volatilisation of Ba as BaH₂O_{2(g)} and BaMoO_{4(g)}.
- At the end of stage 2, 3.7% of the total Ba in the system is in the gas phase, 51.5% is dissolved in the tetragonal ZrO₂ phase, and 44.8% remains in Liquid B.

The Ba present in the gas phase at the end of stage 2 is not considered in the stage 3 calculations. During stage 3, when the atmosphere is switched from oxidizing to reducing, calculations indicate that:

- Ba is exclusively dissolved in ZrO₂-T phase at the beginning of the stage when the oxygen chemical potential of the system drops to -364.8 kJ.mol⁻¹.
- At 1650 °C Ba gradually volatilizes, mainly as BaH₂O_{2(g)} and BaOH_(g), and its dissolved fraction in the (U,Zr)O₂ phase increases.
- Above 1780 °C, as Zr incorporates into the (U,Zr)O₂ phase and ZrO₂-T disappears, BaZrO₃ is formed with a perovskite structure. When the ZrO₂-T phase no longer exists (above 1846 °C), 91.2% of the Ba inventory is found as BaZrO₃, 4.8% in the gas phase, and 4.0% dissolved in the (U,Zr)O₂ phase.
- Above 1850 °C the fraction of Ba in the gaseous phase sharply increases as BaZrO₃ is decomposed, which fully disappears by 2108 °C. At this temperature, 2108 °C, the dissolved fraction of Ba in the ZrO₂-T phase attains its maximum (15.4% of the Ba inventory).
- By the end of stage 3, 4.1% of the total Ba is dissolved in the fluorite phase and the remainder is in the gaseous phase (95.9%), mainly as BaOH_(g), BaO_(g), and BaH₂O_{2(g)}.

The moles of Ba present in the gas phase at the end of stage 3 were not considered for calculations on stage 4. During the latter, from 2400 to 2611 °C, the steam + hydrogen injection was stopped and pure helium flowed through the system. For these conditions, calculations indicate that:

- At the beginning of the stage most of the remaining Ba is in the gas phase (99.2%, mainly as BaO_(g) and Ba_(g)) and 0.8% is dissolved in the (U,Zr)O₂ phase.
- Following the melting of the fuel + oxidized Zircaloy-cladding solution (solid-liquid transition of the (U,Zr)O₂ phase at 2505 °C) a significant amount of Ba is dissolved in the liquid (up to 68.4% of the remaining amount of Ba in stage 4 by 2540 °C).

- At the end of stage 4, 62.2% of Ba is dissolved in Liquid A and the remainder is in the gaseous phase (37.8%).

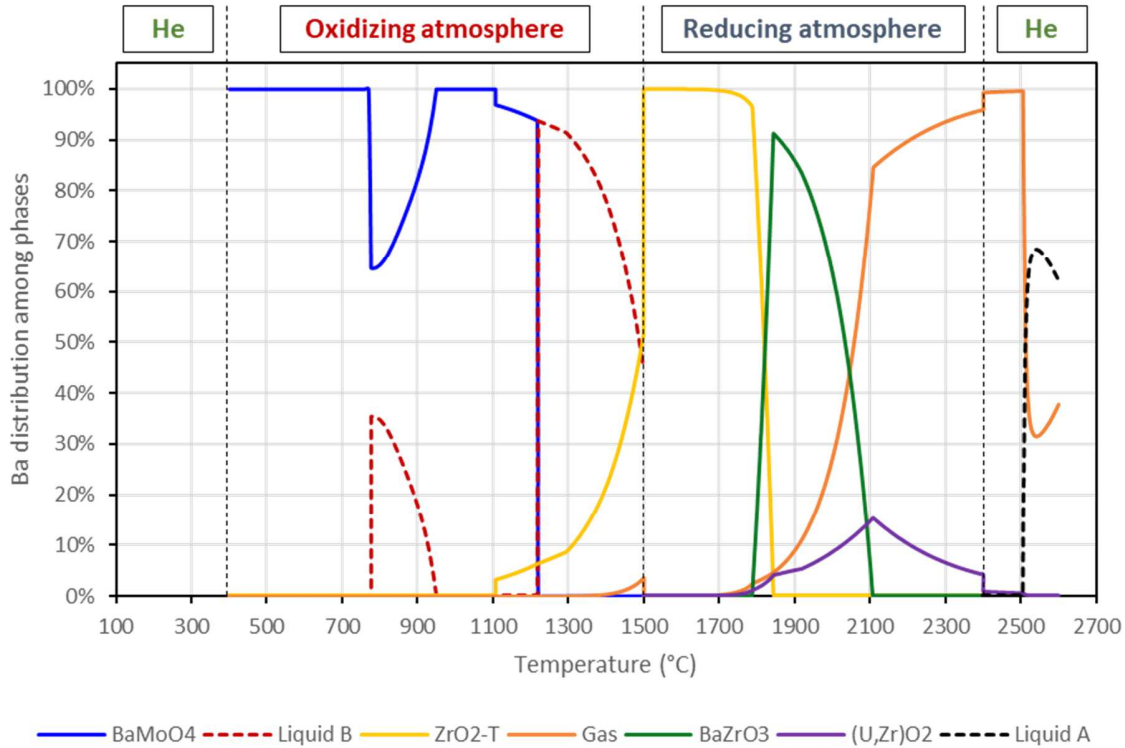


Figure 6: Calculated chemical evolution of barium during the VERDON-1 experiment

Molybdenum

The calculated Mo distribution for stages 2, 3, and 4 is presented in **Figure 7**. According to calculations for stage 2:

- At the beginning of the stage, under an oxidizing atmosphere, Mo is found as MoO_2 (36.2% of the total amount of Mo), BaMoO_4 (32%), $\text{Cs}_2\text{MoO}_4\text{-O}$ (27.9%) and intermetallic phases (3.7%). In order to reduce the complexity of the diagram, the metallic phases in which Mo is present (*e.g.*, MoRh_3 , FCC, and HCP) are grouped together under the title '*metallic phases*'. Although the full composition of these metallic phases and their evolution is not discussed in this work, both the FCC and HCP contain Ru, Rh, Tc, and Pd, and Mo. The evolution of Mo distribution among these phases is presented in **Figure 8**.
- At 776 °C, as observed in the Cs and Ba sections, the $\text{Cs}_2\text{MoO}_4\text{-H}$ phase undergoes a solid-liquid transition and forms Liquid B. Since MoO_2 and BaMoO_4 are dissolved in this liquid phase, the fraction of Mo in the liquid phase (regarding to the total number of Mo moles present in the system) ascends to 41.7%.
- At 950 °C, all Cs_2MoO_4 is in the gaseous phase and Liquid B no longer exists. 32% of Mo is found as BaMoO_4 , 28% in the gaseous phase (as $\text{Cs}_2\text{MoO}_{4(g)}$), 5.6% in the metallic phase, and the balance (34.4%) as MoO_2 . The increased fraction of Mo in the metallic phase corresponds mainly to the reduction of Mo from the MoO_2 phase. As temperature increases during this stage, MoO_2 is further reduced into the metallic phase.

- At 1220 °C, the BaMoO₄ phase undergoes a solid-liquid transition and Liquid B is formed again. As observed, some of the Mo (from the MoO₂ and gaseous phases) is re-dissolved into the liquid.
- At 1295 °C the MoO₂ phase disappears. The Mo from this phase is distributed into the gaseous phase, mainly as MoO_{3(g)} and Mo₂O_{6(g)}, and in the metallic phase.
- Above 1295 °C, the fraction of Mo in the gaseous phase increases because of the volatilization of Mo oxides from Liquid B. At the end of stage 2, 79.9% of Mo is in the gaseous phase, 3.4% in the metallic phase, and 16.7% the liquid phase.

As for the other elements, the amount of Mo present in the gas phase at the end of stage 2 is not considered for calculations for the following stage. During stage 3, when the atmosphere becomes reducing, calculations indicate that:

- Mo is found exclusively in the metallic phase at the beginning of stage 3, in the HCP structure, as observed in **Figure 8**.
- Above 1800 °C the fraction of Mo in the gaseous phase slowly increases, being MoO_{2(g)}, MoO_{3(g)}, MoO_(g), and Mo_(g) the main species.
- Between 2123 and 2160 °C, the metallic HCP phase undergoes a solid-liquid transition and Liquid C is formed, during which the fraction of Mo in the gaseous phase remains constant. The evolution of the composition of the metallic liquid phase is presented in **Figure 9**. At 2160 °C, when the solid metallic phase no longer exists, most Mo is in Liquid C (98% of the total Mo considered for the calculations of this stage) while 2% is in the gaseous phase. The volatilization of Mo from the liquid phase continues as temperature increases. By the end of stage 3, 85.4% of Mo is in the liquid phase and 14.6% is in the gaseous phase.

The fraction of Mo found in the gaseous phase at the end of stage 3 is not considered for the stage 4 calculations. During the last stage of the experiment, where only helium flowed through the system, calculations indicate that 78.2% of the total Mo is dissolved in the metallic Liquid C and 21.8% is in the gaseous phase. The main chemical forms in the latter phase are MoO_{2(g)}, MoO_(g), Mo_(g), and MoO_{3(g)}. The Mo fraction in the gaseous phase increases up to 2505 °C but, when the fluorite phase undergoes a solid-liquid transition and the oxygen chemical potential of the system decreases, a fraction of Mo returns to Liquid C. At the end of this stage, 61.2% of the remaining Mo inventory is found in the gaseous phase (mainly as Mo_(g) and MoO_(g)) and the balance (38.8%) in the liquid phase.

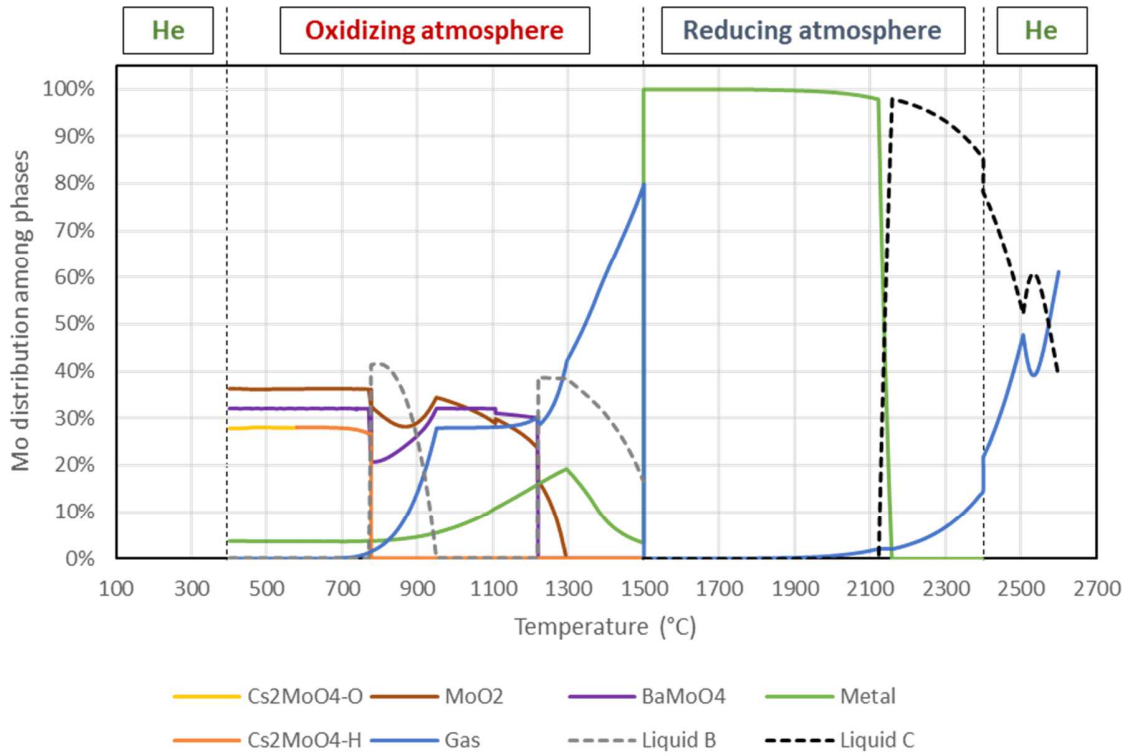


Figure 7: Calculated chemical evolution of molybdenum during the VERDON-1 experiment

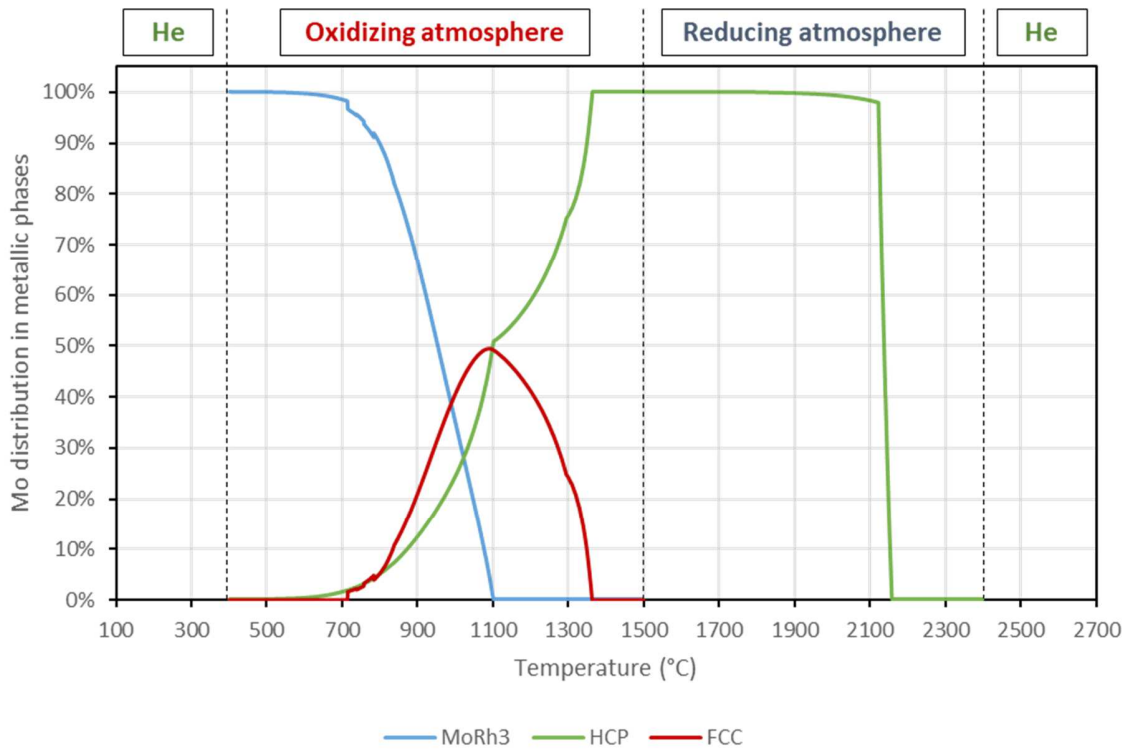


Figure 8: Mo distribution among metallic phases during stages 2 and 3

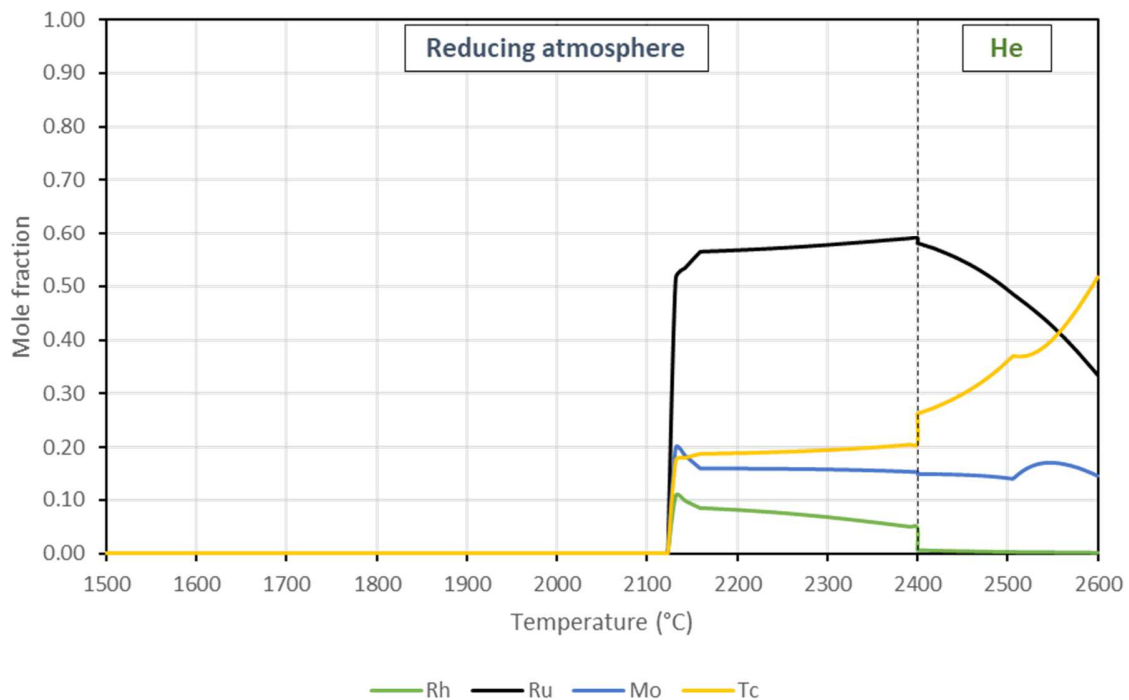


Figure 9: Metallic liquid phase (Liquid C) composition evolution during stages 3 and 4

4.3. OVERALL EVOLUTION OF THE CONDENSED PHASES IN THE IRRADIATED FUEL-CLAD SYSTEM

The calculated number of moles for the phases predicted by the TAF-ID, are represented in **Figures 10 to 12** for illustrative purposes. The primary y-axis of **Figure 10** reports the composition of the major phases, whereas the secondary y-axis reports the evolution of the oxygen-to-metal ratio (O/M) for the fluorite phases (UO_2 and $(\text{U,Zr})\text{O}_2$) and the Liquid A phase (molten fuel + Zircaloy-cladding). The O/M ratio is calculated by considering the main constituents of the phases along with dissolved elements (*i.e.*, O, U, Pu, Nd, Np, Gd, La, and Sr). The O/M ratio of the UO_2 phase (the only fluorite phase during the oxidizing stage) increases up to 2.005 by the end of stage 2 (1500 °C), as observed in **Figure 10**. When the atmosphere is switched to reducing, at the beginning of stage 3, the UO_2 phase becomes slightly hypo-stoichiometric (O/M=1.999). As the experiment progresses, the O/M ratio of both fluorite phases (UO_2 and $(\text{U,Zr})\text{O}_2$) decreases and they become highly hypo-stoichiometric. Finally, Liquid A phase forms during stage 4. The minor phases, such as the many Pd-Te intermetallic compounds formed during stage 2 (up to 900 °C), that highlight the complexity of the system, are represented in **Figure 11** and **Figure 12**. Though the phase transitions and different element interactions are not thoroughly explained to the level above for Ba, Cs, Mo, and Zr, they are summarized in **Table 4**.

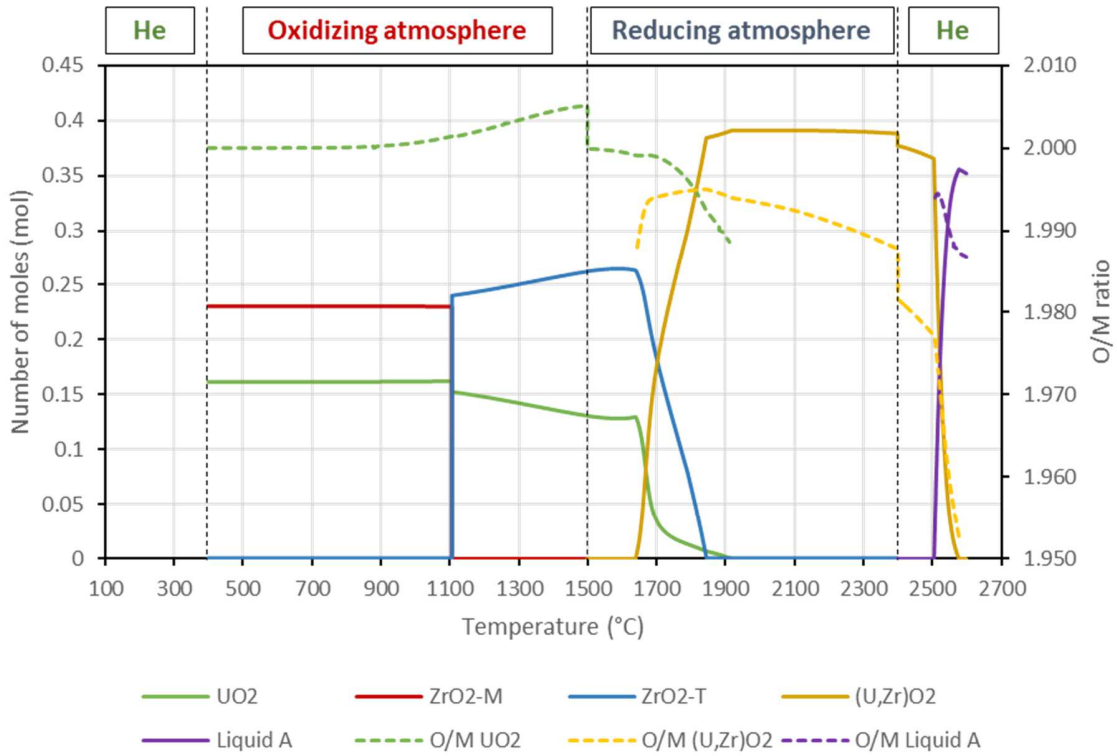


Figure 10: Calculated number of moles of the major phases and O/M ratio

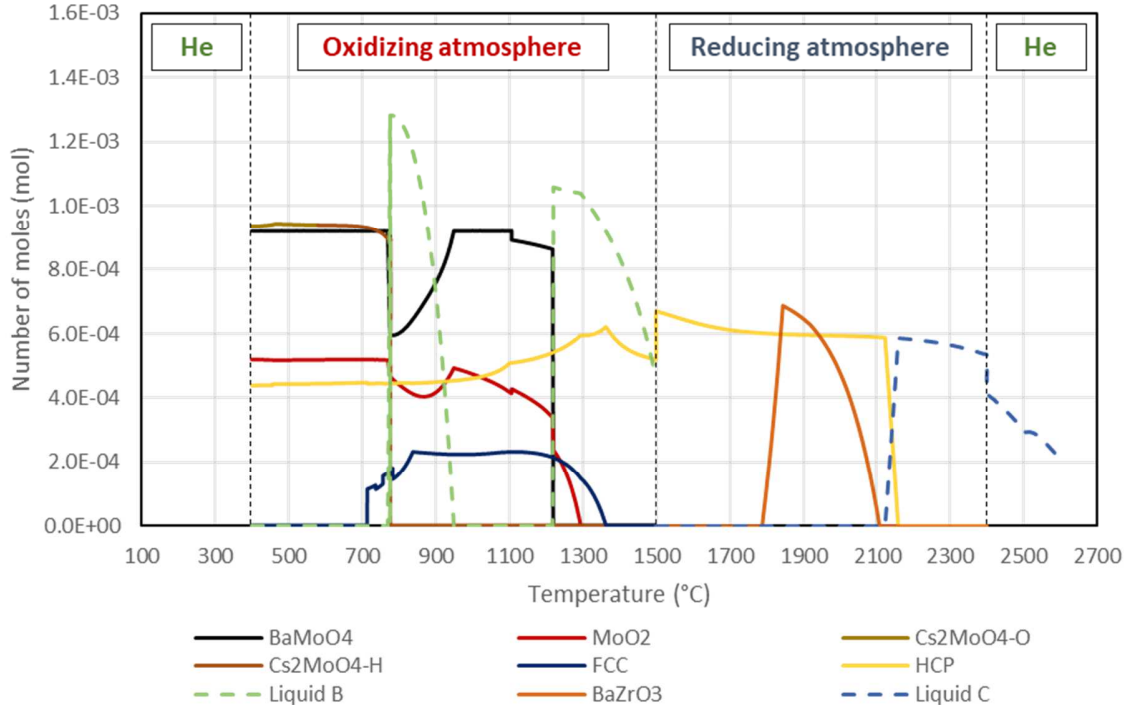


Figure 11: Calculated number of moles of the minor phases (A)

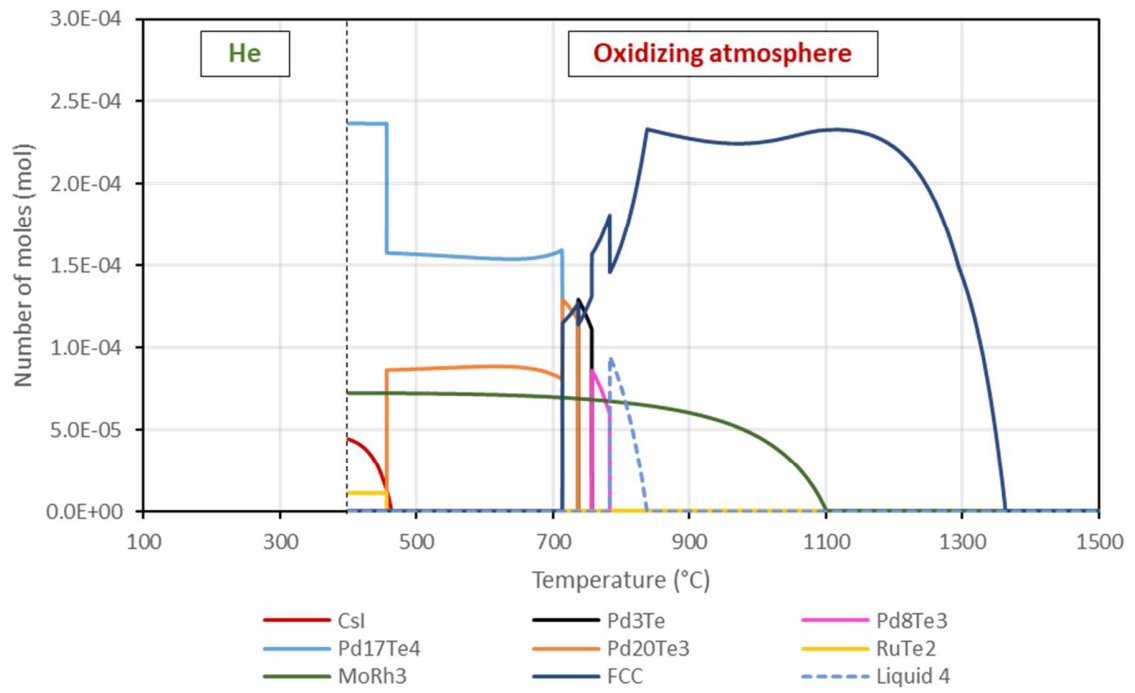


Figure 12: Calculated number of moles of the minor phases (B)

Table 4: Summary of the phase transitions and interactions calculated to occur during the VERDON-1 experiment

	Temperature (°C)	
Stage 2	456	$\text{RuTe}_2 + \text{Pd}_{17}\text{Te}_4 \rightarrow \text{Pd}_{20}\text{Te}_3 + \text{HCP}_{(\text{Ru, Mo, Rh, Pd})}$
	460	$\text{CsI}_{(\text{solid})} \rightarrow \text{CsI}_{(\text{gas})}$
	579	$\text{Cs}_2\text{MoO}_4\text{-Orthorhombic} \rightarrow \text{Cs}_2\text{MoO}_4\text{-Hexagonal}$
	714	$\text{Pd}_{17}\text{Te}_4 \rightarrow \text{Pd}_{20}\text{Te}_3 + \text{FCC}_{(\text{Ru, Mo, Rh, Pd})}$
	737	$\text{FCC}_{(\text{Te, Pd, Rh, Ru, Mo})} + \text{Pd}_{20}\text{Te}_3 \rightarrow \text{PdTe}_3$
	757	$\text{Pd}_3\text{Te} \rightarrow \text{Pd}_8\text{Te}_3 + \text{FCC}_{(\text{Ru, Mo, Rh, Pd})}$
	776	$\text{Cs}_2\text{MoO}_4\text{-Hexagonal} + \text{BaMoO}_4 + \text{MoO}_2 \rightarrow \text{Liquid B}_{(\text{Ba, Cs, Mo, O})}$ The solid-liquid transition of $\text{Cs}_2\text{MoO}_4\text{-H}$ triggers the formation of Liquid B. BaMoO_4 and MoO_2 are partially dissolved in the latter
	783	$\text{FCC}_{(\text{Te, Pd, Rh, Ru, Mo})} + \text{Pd}_8\text{Te}_3 \rightarrow \text{Liquid D}_{(\text{Te, Pd})}$
	830	$\text{Liquid D}_{(\text{Te, Pd})} \rightarrow \text{FCC}_{(\text{Te, Pd, Rh, Ru, Mo})} + \text{HCP}_{(\text{Pd, Rh, Mo, Ru, Tc})}$
	950	$\text{Liquid B} \rightarrow \text{Cs}_2\text{MoO}_{4(\text{gas})} + \text{BaMoO}_{4(\text{s})} + \text{MoO}_{2(\text{s})}$
	1105	$\text{ZrO}_2\text{-Monoclinic} \rightarrow \text{ZrO}_2\text{-Tetragonal}$ $\text{BaMoO}_4 + \text{ZrO}_2\text{-Tetragonal} \rightarrow \text{Ba}_{(\text{ZrO}_2\text{-T})} + \text{BaMoO}_4 + \text{MoO}_2$ $\text{MoRh}_3 \rightarrow \text{FCC}_{(\text{Te, Pd, Rh, Ru, Mo})} + \text{HCP}_{(\text{Pd, Rh, Mo, Ru, Tc})}$
	1220	$\text{BaMoO}_4 + \text{Cs}_2\text{MoO}_{4(\text{g})} + \text{MoO}_2 \rightarrow \text{Liquid B}_{(\text{Ba, Cs, Mo, O})}$ The solid-liquid transition of BaMoO_4 triggers the formation of Liquid B. MoO_2 and $\text{Cs}_2\text{MoO}_{4(\text{g})}$ are partially dissolved in the latter.
	1295	$\text{MoO}_2 \rightarrow \text{Mo}_{(\text{HCP})} + \text{MoO}_{3(\text{gas})} + \text{Mo}_2\text{O}_{6(\text{gas})} + \text{Mo}^{2+}_{(\text{Liquid B})}$
	1360	$\text{FCC}_{(\text{Mo, Pd, Rh, Ru, Tc, Te})} \rightarrow \text{Te}_{(\text{gas})} + \text{HCP}_{(\text{Mo, Ru, Rh, Pd, Tc})}$
Stage 3	1675	$\text{ZrO}_2\text{-Tetragonal} + \text{UO}_2 \rightarrow (\text{U, Zr})\text{O}_2$ This reaction is progressive, by 1920 °C $\text{ZrO}_2\text{-T}$ and UO_2 form a single $(\text{U, Zr})\text{O}_2$ phase
	1788	$\text{Ba}_{(\text{ZrO}_2\text{-T})} \rightarrow \text{BaZrO}_3(\text{Perovskite})$
	2108	$\text{BaZrO}_3(\text{Perovskite}) \rightarrow \text{BaO}_{(\text{g})} + \text{Ba}_{((\text{U, Zr})\text{O}_2)}$
	2123	$\text{HCP}_{(\text{Mo, Ru, Tc, Rh})} \rightarrow \text{Liquid C}_{(\text{Mo, Ru, Tc, Rh})}$
Stage 4	2505	$(\text{U, Zr})\text{O}_2 \rightarrow \text{Liquid A}_{(\text{U, Zr, O})}$

5. COMPARISON TO EXPERIMENTAL OBSERVATIONS AND DISCUSSION

As indicated in the introduction of this manuscript, the experimental observations completed during the VERDON-1 experiment included gamma spectrometry measurements and post-mortem sample chemical characterisations. In this section, the experimental results available in [6–8] are compared to the calculation results presented in the preceding sections. Particularly: (i) the release behaviour of Ba, Cs, I, Mo, and Zr, (ii) the $\text{UO}_2\text{-ZrO}_2$ interactions that led to the sample melting by the end of the experiment, and (iii) the chemical state of Mo, Ba, and Zr in the sample at the end of the experiment.

5.1. RELEASE BEHAVIOUR OF BA, CS, I, MO, AND ZR

The measured release fractions of Ba, Cs, I, Mo, and Zr during the VERDON-1 experiment are presented in **Figure 13** from Ref. [8].

During the VERDON-1 experiment it was observed that:

- During stage 2, Cs, I, and Mo release started simultaneously during the oxidation plateau at 1500 °C. At the end of the oxidizing stage, Cs and I released fractions were approximately 60% and Mo released fraction was approximately 40%.
- At the beginning of stage 3, under reducing atmosphere the Mo release stopped. Cs and I continued to be released together in steps, following the temperature ramps and plateaus. Ba release started at approximately 1800 °C and reached a total released fraction of 60% by the end of stage 3 (2400 °C).
- During stage 4, under neutral atmosphere, Cs and I release continued and were both completely released by the end of the stage. Ba and Mo were also further released, reaching released fractions of 75% and 60%, respectively. No release of Zr was observed during the whole experiment.

The evolution of Ba, Cs, I, Mo, and Zr fraction in gaseous state with temperature, calculated with the TAF-ID for the different stages of the VERDON-1 experiment, is presented in **Figure 14**.

During stage 2, calculations predict that:

- Iodine is the first element to become volatile (465 °C).
- A fraction of Cs becomes volatile together with iodine and the rest of the Cs follows into the gaseous phase because of the destruction of the Cs_2MoO_4 phase above 700 °C. A fraction of Cs is dissolved in the liquid phase formed by the solid-liquid transition of BaMoO_4 at 1220 °C. However, by the end of the experiment all the Cs in the system is found in the gaseous phase.
- Mo fraction in gaseous state increases from 1290 °C and attains 79.9% by the end of the oxidation plateau.

TAF-ID calculations predicted an earlier release of Cs, I, and Mo than the one observed experimentally. Nevertheless, during the experiment these three elements were suddenly released at the same time during the oxidation plateau. Two different hypotheses have been proposed to explain this behaviour:

- The sudden release of these elements would imply that they were already in the gaseous phase during the oxidation plateau, but contained by the Zircaloy-cladding. Once the Zircaloy-cladding was fully oxidized and failed, these elements were released [20–23]. Knudsen Effusion Mass Spectrometry (KEMS) experiments done on oxidized and un-cladded irradiated fuel elements have showed an earlier fission products release [9,24] in line with TAF-ID calculations, which supports this hypothesis.
- The interconnection of pores in the fuel matrix would take place at temperatures close to that of the oxidation plateau [6,7] allowing the release of gaseous species from the fuel.

A combination of these two phenomena could explain the sudden release of these species which present very different volatilities, and the difference observed between experimental and calculation results. The shape of the experimental release profiles of Cs and I in **Figure 13**, after the oxidation plateau, can be attributed to the diffusion of the gaseous species in the fuel matrix.

Cs and Mo release during the VERDON-1 experiment has been previously analysed in Ref. [25]. In the latter work, authors attributed the Cs and Mo behaviour observed experimentally to the existence of the $\text{Cs}_2\text{Mo}_2\text{O}_{7(g)}$ gaseous species instead of $\text{CsMoO}_{4(g)}$ only, based on the results presented in Ref. [26]. Results

presented in [25] are interesting and it is agreed that an element's diffusion inside the fuel matrix plays an important role on their release. However, the authors of the present manuscript do not completely agree on the existence of $\text{Cs}_2\text{Mo}_2\text{O}_7(\text{g})$ as the results presented in [26] are not conclusive. Therefore, additional experimental data should be collected to probe the existence of $\text{Cs}_2\text{Mo}_2\text{O}_7(\text{g})$ or ab-initio calculations conducted in order to determine the stability of this molecule in the gaseous phase. Also, it should be noted that $\text{Cs}_2\text{Mo}_2\text{O}_7$ and other higher caesium molybdates are not yet described in the current version of the TAF-ID.

During stage 3, under reducing atmosphere, calculations indicate that:

- Mo would only exist in a metallic phase at the beginning of the stage. By the end of stage 3, the calculated Mo fraction in the gaseous phase is 14.6%.
- Ba fraction in the gaseous phase starts increasing from 1680 °C, but becomes significant only after 1800 °C.

Both calculation results were in good agreement with the experimental observations. Indeed, during the VERDON-1 experiment, it was observed that Mo release stopped at the beginning of the third stage under a reducing atmosphere. Mo condensation into a metallic phase would explain the plateau observed on its experimental released fraction. As for Ba, both experimental and calculation results indicate that its released fraction was significant above 1800 °C.

During stage 4, it was observed experimentally that Mo released fraction increased as soon as the steam-hydrogen flow was stopped, and continued to increase until the end of the experiment. This observation was in good agreement with calculations as Mo fraction in the gas phase was predicted to increase with this atmosphere change. Also, it was predicted that a fraction of Mo would condense during the solid-liquid transition of the (U,Zr) O_2 phase and consequent oxygen potential decrease. Experimentally, a slight decrease of Mo release would be expected during the solid-liquid transition, though such behaviour was not observed. In a similar way, calculations predicted that Ba would also condense because of the oxygen potential drop, which would be observed experimentally as a sudden stop in Ba release. Again, such behaviour was not observed experimentally. Nevertheless, according to experimental results the solid-liquid transition of the sample did not occur until the end of the experiment, so the release behaviour predicted by calculations would be delayed. As for zirconium, no release was measured during the whole experiment, which was in good agreement with calculations (only 0.3% of the whole Zr inventory was predicted to be in the gaseous phase at the end of stage 4).

The calculated release fractions of the elements were systematically overestimated by the thermodynamic calculations. This result was expected, as the kinetic release mechanisms have not been considered. Nevertheless, the tendencies of the release evolution of the elements as a function of temperature and oxygen potential are well explained by the calculations. Hence, a qualitative agreement was obtained.

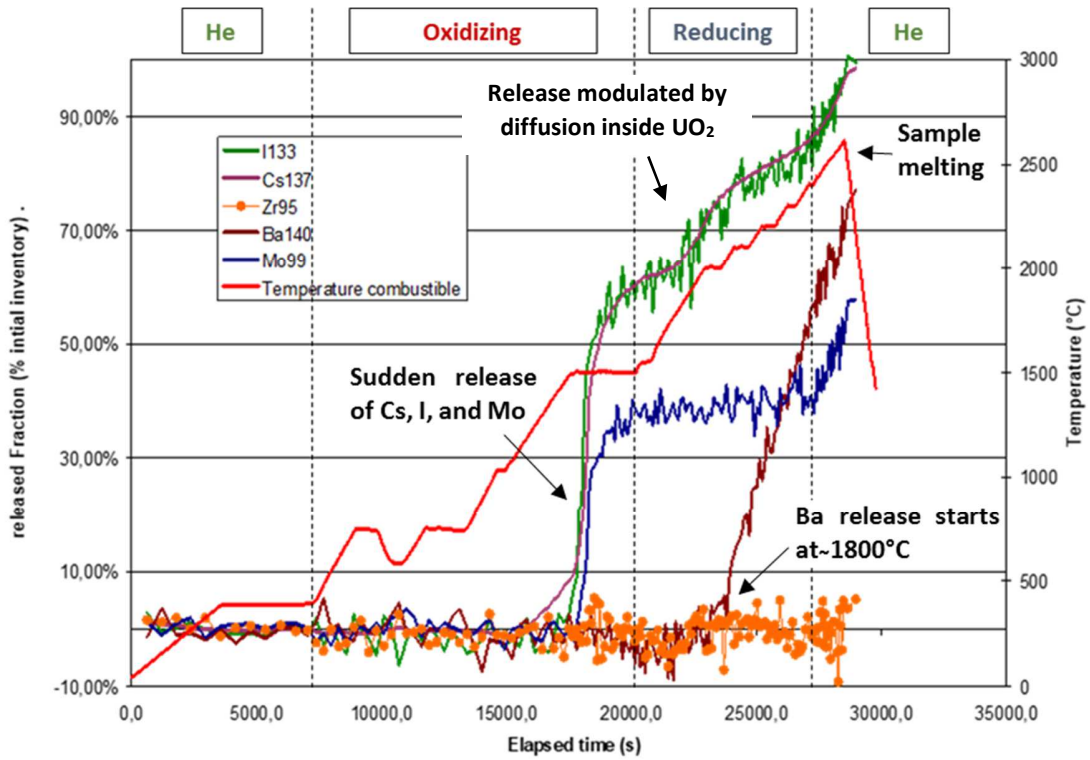


Figure 13: Ba, Cs, I, Mo, and Zr released fractions measured during the VERDON-1 experiment [5]

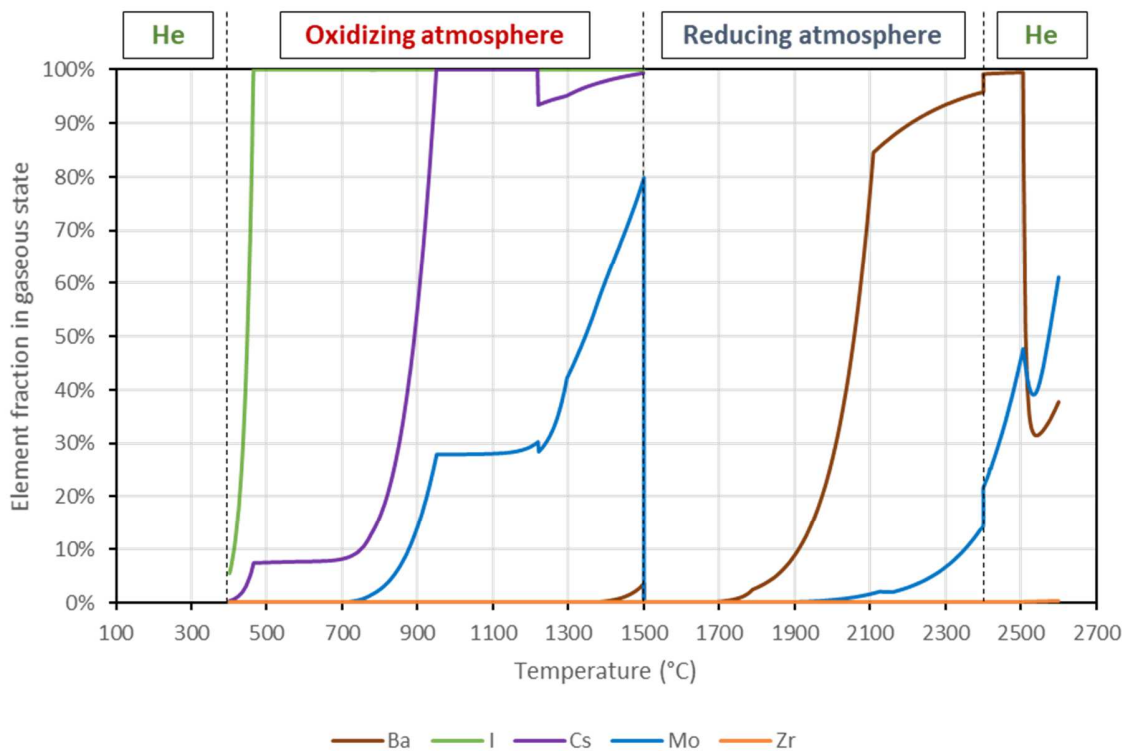


Figure 14: Calculated Ba, Cs, I, Mo, and Zr elemental fractions of the gas phase for the VERDON-1 experiment

5.2. SAMPLE MELTING BY THE END OF THE EXPERIMENT

A SEM-SE image of one of the irradiated pellets of the VERDON-1 sample is presented in **Figure 15**. As discussed in Ref. [6], the dark-grey region (elevated-porosity) corresponds to the UO_2 matrix whereas the two light-grey regions (moderate and low porosity, respectively) correspond to a $(\text{U,Zr})\text{O}_2$ phase. Ref. [6] concluded that the oxidized Zircaloy-cladding dissolved the periphery of the sample and melted, penetrating the sample through the cracks. At the same time, the liquid diffused through the UO_2 structure producing two different light-grey regions with different porosities. The characteristics of these regions are observed in **Figure 16**, where dashed lines highlight the different zones. **Figure 17** shows the quantitative results on the O, Zr, U, and Pu composition for the different porosity regions for the line scan depicted in **Figure 16**.

These results highlight the different U and Zr concentration in the three regions:

- The elevated porosity region is fuel unaffected by the oxidized Zircaloy-cladding, corresponding to UO_2 containing a small fraction of Zr;
- The moderate porosity region is a transition zone where Zr was diffusing in the UO_2 matrix forming a mixed oxide with a maximum Zr content of $(\text{U}_{0.75}\text{Zr}_{0.25})\text{O}_{2-x}$ when the experiment was stopped; and
- The reduced porosity region is the oxidized Zircaloy-cladding with dissolved U, with a composition close to $(\text{U}_{0.5}\text{Zr}_{0.5})\text{O}_{2-x}$, mainly from the periphery of the fuel, which is supported by the increased Pu content, as observed in **Figure 17**.

Despite it is clear that the sample was not in thermodynamic equilibrium during the experiment, there is good agreement between the thermodynamic calculations and the experimental observations (*e.g.*, calculations predicted that the $(\text{U,Zr})\text{O}_2$ phase would melt at 2505 °C). Nevertheless, it must be highlighted that fragments of the Zircaloy-cladding were recovered along with the fuel samples after the VERDON-1 experiment, and therefore not all of the Zircaloy-cladding interacted with the fuel during the experiment.

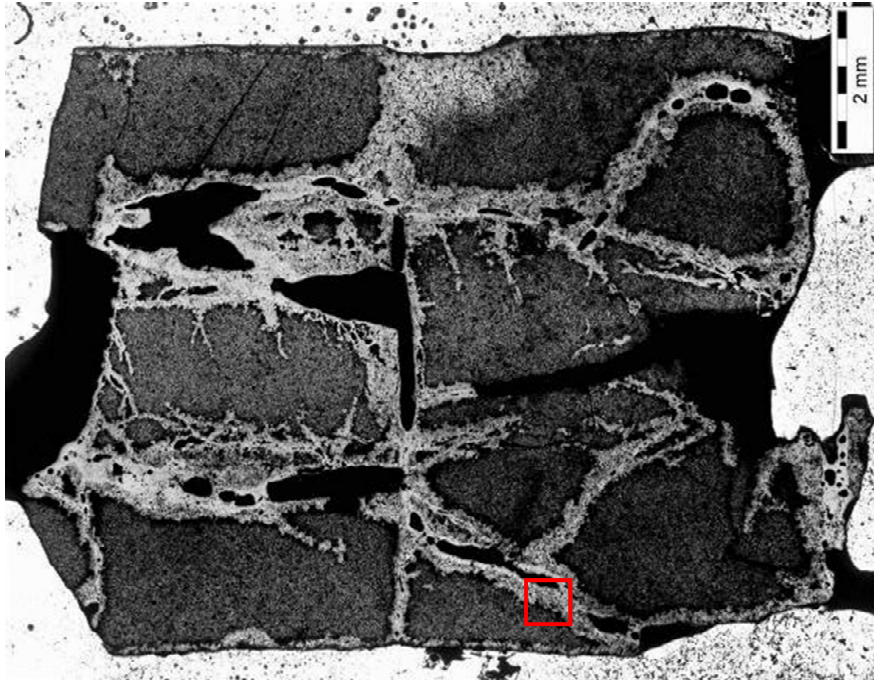


Figure 15: SEM-SE image of an irradiated fuel pellet after the VERDON-1 experiment [6]

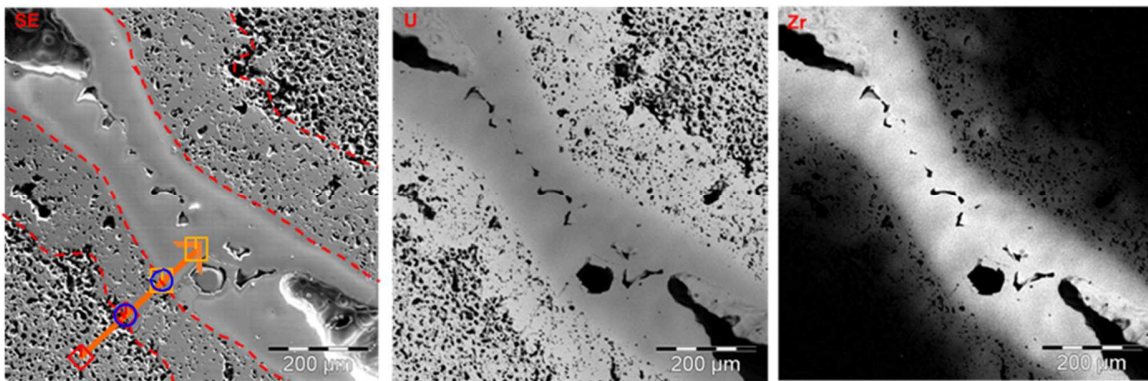


Figure 16: SEM-SE image and corresponding zirconium and uranium X-ray maps acquired on an irradiated fuel pellet post VERDON-1 experiment [6], at the position indicated in Figure 15.

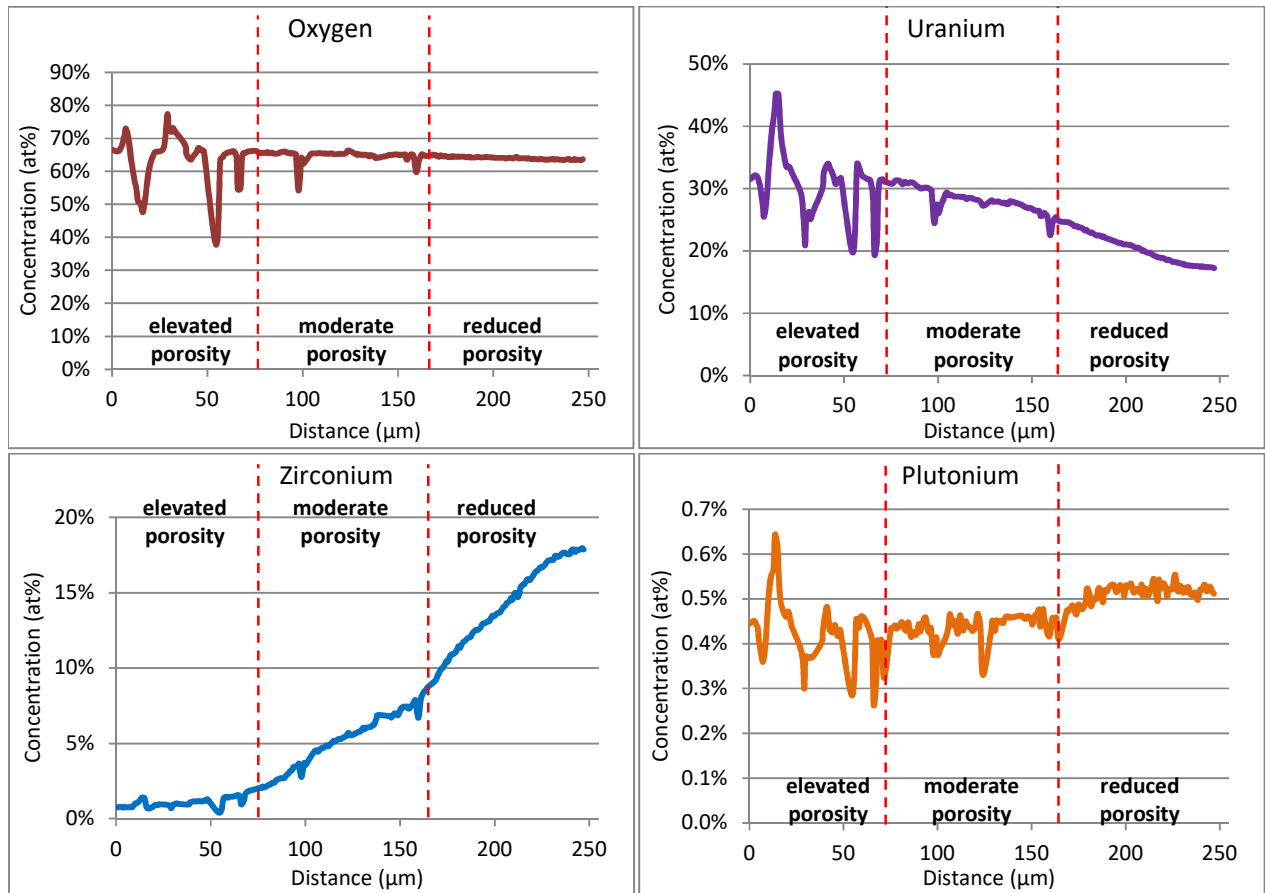
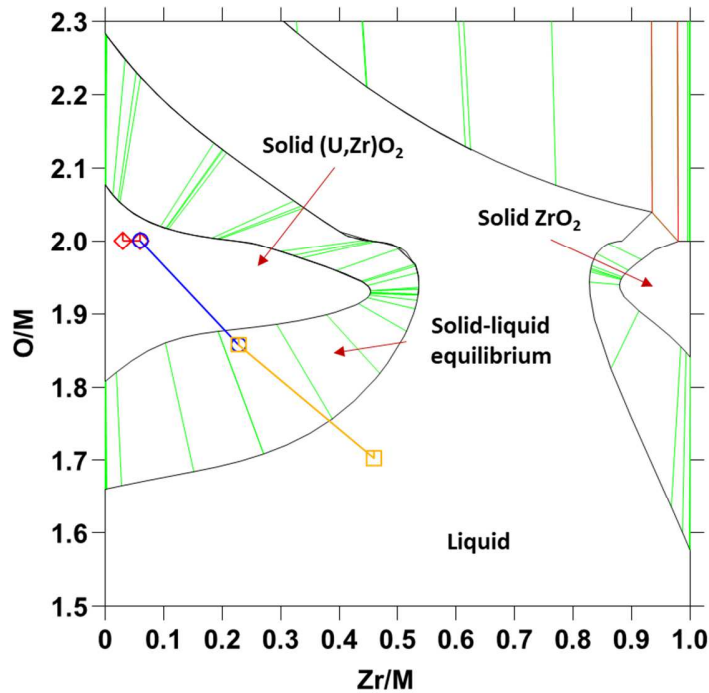


Figure 17: Quantitative results for O, U, Zr and Pu post VERDON-1 experiment sample [6]. *Note, the discontinuities observed (peaks) are related to the porosity of the sample.*

The U-Zr-O ratios determined experimentally at the boundaries of each porosity region indicated in **Figure 17** are represented in the U-Zr-O ternary isothermal section in **Figure 18**, which has been calculated using the TAF-ID. As observed, the ratios measured at the high porosity region correspond to solid UO_2 . In the moderate porosity region, as the O/M ratio decreases and the matrix becomes richer in Zr, the system composition approaches the solid-liquid equilibrium of $(\text{U,Zr})\text{O}_2$ in the ternary diagram. Towards the centre of the reduced porosity region, the ratios measured correspond to hypo-stoichiometric $(\text{U,Zr})\text{O}_2$ in equilibrium with a liquid phase with a decreasing O/M ratio. These results are also in good agreement with experimental observations, as they show that a diffusion path existed between the UO_2 fuel matrix and a reduced liquid phase with a composition close to $(\text{U}_{0.5}\text{Zr}_{0.5})\text{O}_{2-x}$. According to the calculations, the whole system (irradiated fuel + Zircaloy-cladding) is fully molten at 2611 °C, which is not the observed case presumably because the system did not reach chemical equilibrium during the experiment.



◇ UO_2 elevated porosity
○ $(\text{U,Zr})\text{O}_2$ moderate porosity
□ $(\text{U,Zr})\text{O}_2$ reduced porosity

Figure 18: U-Zr-O diagram calculated with the TAF-ID at 2611 °C. Note, that the M denotes the sum of the U and Zr mole fractions.

Figure 19 presents the solidification path of a system consisting of U, Zr, and O with concentrations matching the ones measured at the centre of the reduced porosity region. According to this diagram, a single liquid phase exists above 2611 °C, but as soon as the temperature decreases a solid fluorite solution of $(\text{U,Zr})\text{O}_2$ is formed. The solid and liquid phases are in equilibrium down to 1830 °C, at which point a metallic phase with HCP structure is formed (68 at% Zr, 2 at% U, and 30 at% O). At lower temperatures, the uranium content in the HCP metallic phase becomes negligible. Below 1463 °C a miscibility gap appears in the $(\text{U,Zr})\text{O}_2$ solution and UO_2 is formed. At 1356 °C the $(\text{U,Zr})\text{O}_2$ phase no longer exists as it decomposes into tetragonal ZrO_2 and UO_2 . Nevertheless, uranium is still soluble in the tetragonal ZrO_2 phase. At 1108 °C there is a transition in the ZrO_2 phase from tetragonal to monoclinic and the phase fraction of UO_2 increases as uranium is insoluble in monoclinic ZrO_2 . Therefore, according to calculations three main phases would be in equilibrium at room temperature in the reduced porosity region: (i) UO_2 , (ii) monoclinic ZrO_2 , and (iii) metallic HCP Zr. However, these calculation results cannot be confirmed as X-ray maps presented for the reduced porosity region (**Figure 16**) can only confirm that the region is not completely homogeneous.

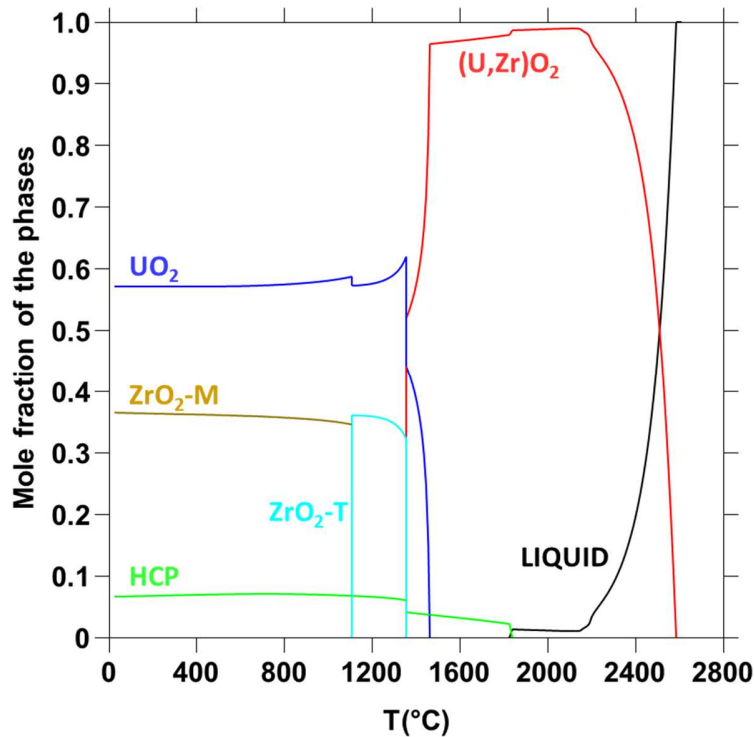


Figure 19: Solidification path of the reduced porosity (U,Zr)O₂ region

5.3. CHEMICAL STATE OF MO, BA, AND ZR IN THE POST-MORTEM SAMPLE

Barium and zirconium

Calculations showed that, at the beginning of stage 4, all Ba was in the gaseous phase as BaO_(g) and Ba_(g). Part of the Ba in the latter was dissolved in the liquid phase formed by the melting of the (U,Zr)O₂ phase at 2505 °C. These results are in good agreement with experimental observations, as the Ba and Zr X-ray maps (**Figure 20**) acquired in the elevated porosity region, unaffected by the oxidized Zircaloy-cladding, indicate that very few precipitates of these elements remain. Furthermore, Ba was no longer associated to Zr. This supports the calculation results indicating that Ba was being released during stage 4 as BaO_(g) and Ba_(g). Furthermore, no Ba or Zr precipitates were observed in the X-ray maps for the moderate porosity region (**Figure 21**), which indicate that Ba was dissolved into the forming liquid phase. The Ba concentration in the different regions could not be determined experimentally since the signal was low and close to the detection limit of the instrument.

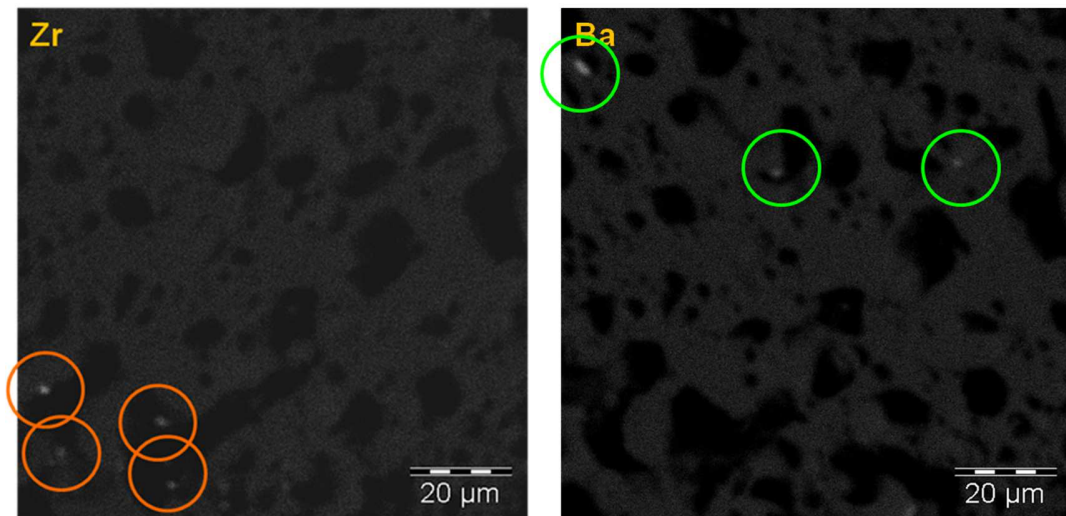


Figure 20: Zr (left) and Ba (right) X-ray maps acquired in the elevated-porosity region [8]

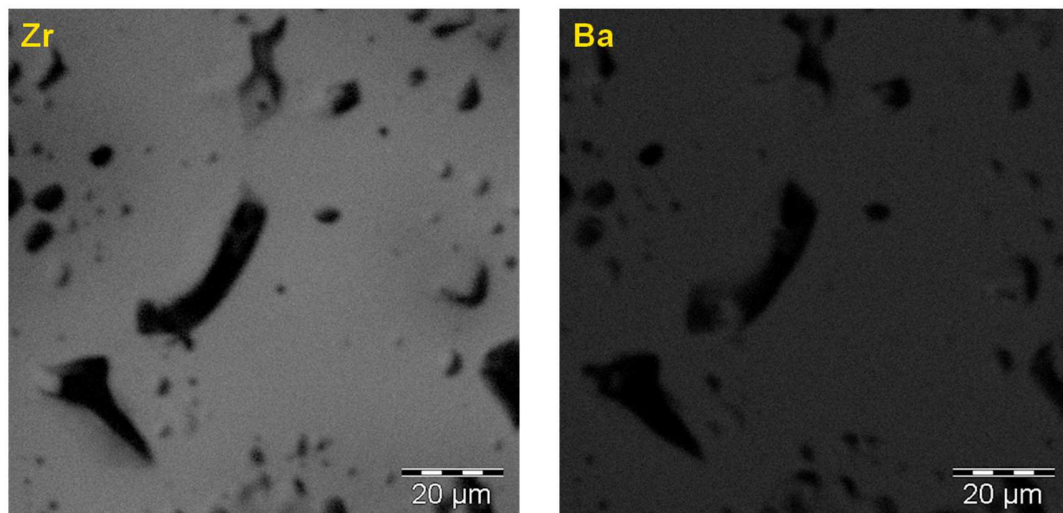


Figure 21: Zr (left) and Ba (right) X-ray maps acquired in the moderate-porosity region [8]

Molybdenum

During stage 4 of the VERDON-1 experiment, calculations indicate that Mo exists in the gaseous phase as different oxides and in the metallic liquid phase as well. The calculated evolution of the composition of the metallic liquid phase during stage 4 is presented in **Figure 22**. The composition is presented in wt%, for ease of comparison with experimental results available in [7]. As observed, Ru, Tc, and Mo are the main constituents of the metallic liquid phase. Calculations predict that both Mo and Ru would volatilize and so their concentration decreases as temperature increases, whereas the Tc amount the liquid phase remains unchanged and hence its concentration increases. Nevertheless, Tc is only described in metallic state in the current version of the TAF-ID and therefore no volatilisation from the oxidation of this element is calculated.

Experimentally, two metallic precipitates have been characterised in the VERDON-1 sample after the experiment, through EPMA quantitative line scans. These results correspond to metallic precipitates found in the periphery (**Figure 23 A**) and centre (**Figure 23 B**) of the sample. In both cases it was observed that

Ru, Tc, and Mo are the main constituents. Also, Rh and Pd were present, but in lower concentrations. Though there was a good agreement between the calculated and experimentally observed concentrations, the thermodynamic calculations estimate a lower concentration of Ru by the end of stage 4. This could be attributed either to an overestimation on the calculated fraction of gaseous Ru or to phenomena during the VERDON-1 experiment that retained Ru gaseous species.

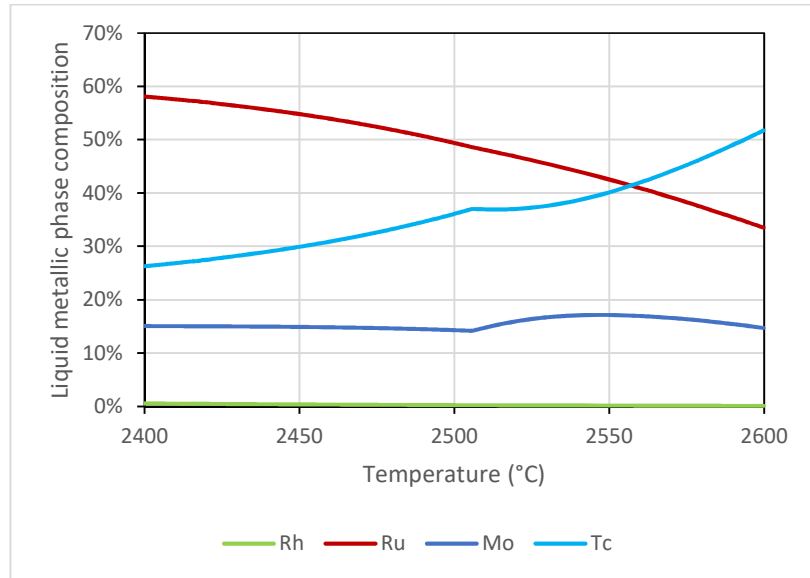


Figure 22: Calculated composition evolution of the metallic liquid during stage 4

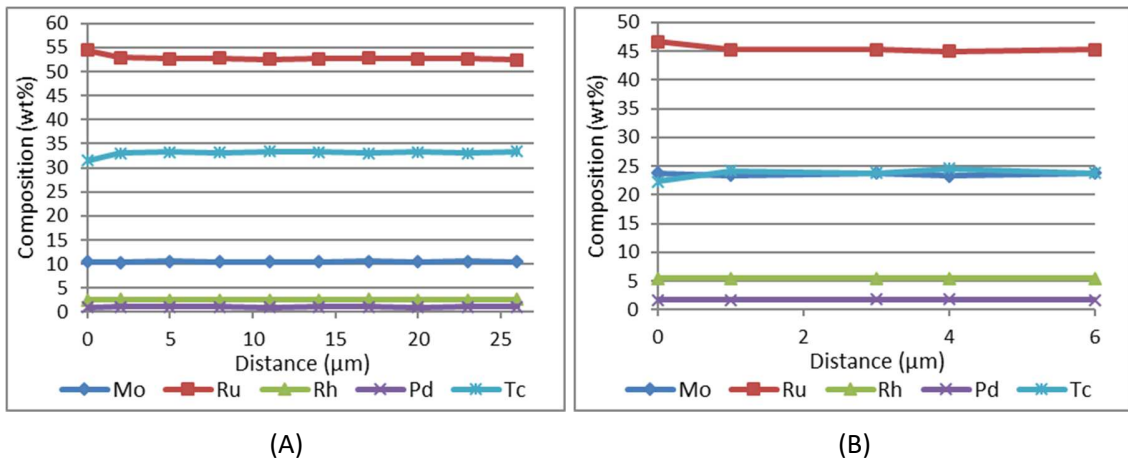


Figure 23: Quantitative results of the metallic precipitates found at the periphery (A) and centre (B) of the sample [7]

6. CONCLUSIONS

The distribution of 15 elements and particularly of Ba, Cs, I, Mo, and Zr, in the different phases (gas, solid, and liquid) during the VERDON-1 experiment, which simulated a nuclear severe accident sequence, has been calculated using the TAF-ID database. Results have been compared to: (i) the release kinetics determined by on-line gamma spectrometry during the experiment and (ii) post-experiment measurements completed on the sample.

Though experimental observations clearly indicate that the VERDON-1 sample was not in thermodynamic equilibrium and that some phenomena cannot be reproduced by these calculations (*e.g.*, Zircaloy-cladding containment effects, pores interconnection, kinetic effects, *etc.*), the overall behaviour of the studied fission products was qualitatively well reproduced with the TAF-ID thermodynamic equilibrium calculations. More specifically, the TAF-ID calculations allowed explaining the following experimental observations:

- High temperature fuel melting behaviour: TAF-ID calculations help explain the interactions between the fuel and the oxidized Zircaloy-cladding that led to the melting of a part of the sample during the final stage of the VERDON-1 experiment. The calculated results presented in this manuscript support the hypothesis that a $(U,Zr)O_{2-x}$ phase was formed due to the interaction with the oxidized Zircaloy-cladding, which melted at high temperature. The calculated temperature of the liquid phase formation was in good agreement with experimental observations. Again, it must be emphasized that not all the Zircaloy-cladding reacted with the UO_2 fuel as cladding fragments were recovered after the experiment.
- Evolution of Mo and Ba: TAF-ID results explain the release behaviour of Mo and Ba elements. For example, calculations were able to reproduce the observed behaviour in stage 2 where Mo release stopped when the atmosphere was switched from oxidizing to reducing. Further, TAF-ID calculations were able to reproduce the restart of Mo release at higher temperatures. Similarly, the release of Ba during stage 3 (high temperature reducing atmosphere) was well reproduced.

In conclusion, the calculations using the TAF-ID, in its current degree of development, allow an overall good prediction of the complex chemistry of irradiated nuclear fuel and its interaction with the Zircaloy-cladding under accident conditions. Further work on the TAF-ID development is directed towards the inclusion of missing systems (*e.g.*, Mo-Sr-O), and calculations on other complex systems involving nuclear materials (*e.g.*, VERDON or VERCORS experiments). Finally, the future coupling of the TAF-ID to fuel performance and/or severe accident codes will be an important step towards the accurate prediction of all phenomena present in severe accident scenarios.

7. ACKNOWLEDGEMENTS

The authors acknowledge financial support from the Natural Sciences and Engineering Research Council of Canada (NSERC), the CANDU Owners' Group (COG), and the University Network of Excellence in Nuclear Engineering (UNENE) through Grant No. NSERC CRD 428829-2011. Also, authors acknowledge and thank Bonnie Brusewitz Lindahl for her contribution with thermodynamic calculations.

8. DATA AVAILABILITY

The raw/processed data required to reproduce these findings (other than the input data for thermodynamic calculations that is provided in section 3) cannot be shared at this time due to legal or ethical reasons.

9. REFERENCES

- [1] NEA Nuclear Science Committee - Thermodynamics of Advanced Fuels – International Database (TAF-ID), (n.d.). <https://www.oecd-nea.org/science/taf-id/> (accessed September 4, 2017).
- [2] C. Guéneau, S. Gossé, A. Quaini, N. Dupin, B. Sundman, M. Kurata, T.M. Besmann, P.E.A. Turchi, J.C. Dumas, E.C. Corcoran, M.H.A. Piro, T. Ogata, R. Hania, B.O. Lee, R. Kennedy, S. Massara, FUELBASE,

TAF-ID Databases and OC Software: Advanced Computational Tools to Perform Thermodynamic Calculations on Nuclear Fuel Materials, (2015). http://www.sar-net.eu/sites/default/files/ERMSAR_2015/Papers/In-vessel_corium/065_Gueneau_final.pdf.

- [3] N. Saunders, A.P. Miodownik, CALPHAD (Calculation of Phase Diagrams): A Comprehensive Guide, Elsevier, 1998.
- [4] Y. Pontillon, A. Gallais-During, International Source Term Program - VERDON-1 Test: Fission Product release from a High Burn-up UO₂ fuel in Severe Accident Conditions: Final Report, CEA, Cadarache, France, 2012.
- [5] Y. Pontillon, E. Geiger, C. Le Gall, S. Bernard, A. Gallais-During, P.P. Malgouyres, E. Hanus, G. Ducros, Fission products and nuclear fuel behaviour under severe accident conditions part 1: Main lessons learnt from the first VERDON test, *J. Nucl. Mater.* 495 (2017) 363–384. doi:10.1016/j.jnucmat.2017.08.021.
- [6] E. Geiger, C. Le Gall, A. Gallais-During, Y. Pontillon, J. Lamontagne, E. Hanus, G. Ducros, Fission products and nuclear fuel behaviour under severe accident conditions part 2: Fuel behaviour in the VERDON-1 sample, *J. Nucl. Mater.* 495 (2017) 49–57. doi:10.1016/j.jnucmat.2017.08.002.
- [7] C. Le Gall, E. Geiger, A. Gallais-During, Y. Pontillon, J. Lamontagne, E. Hanus, G. Ducros, Fission products and nuclear fuel behaviour under severe accident conditions part 3: Speciation of fission products in the VERDON-1 sample, *J. Nucl. Mater.* 495 (2017) 291–298. doi:10.1016/j.jnucmat.2017.08.001.
- [8] E. Geiger, Study of Fission Products (Cs, Ba, Mo, Ru) behaviour in irradiated and simulated Nuclear Fuels during Severe Accidents using X-ray Absorption Spectroscopy, SIMS and EPMA, phdthesis, Université Paris-Saclay, 2016. <https://tel.archives-ouvertes.fr/tel-01309027/document> (accessed January 16, 2018).
- [9] R.J.M. Konings, T. Wiss, O. Beneš, Predicting material release during a nuclear reactor accident, *Nat. Mater.* 14 (2015) 247–252. doi:10.1038/nmat4224.
- [10] M.S. Veshchunov, V.D. Ozrin, V.E. Shestak, V.I. Tarasov, R. Dubourg, G. Nicaise, Development of the mechanistic code MFPR for modelling fission-product release from irradiated UO₂ fuel, *Nucl. Eng. Des.* 236 (2006) 179–200. doi:10.1016/j.nucengdes.2005.08.006.
- [11] P. Chatelard, N. Reinke, S. Arndt, S. Belon, L. Cantrel, L. Carenini, K. Chevalier-Jabet, F. Cousin, J. Eckel, F. Jacq, C. Marchetto, C. Mun, L. Piar, ASTEC V2 severe accident integral code main features, current V2.0 modelling status, perspectives, *Nucl. Eng. Des.* 272 (2014) 119–135. doi:10.1016/j.nucengdes.2013.06.040.
- [12] E.C. Corcoran, M.H. Kaye, M.H.A. Piro, An overview of thermochemical modelling of CANDU fuel and applications to the nuclear industry, *Calphad.* 55 (2016) 52–62. doi:10.1016/j.calphad.2016.04.010.
- [13] M.H.A. Piro, J. Banfield, K.T. Clarno, S. Simunovic, T.M. Besmann, B.J. Lewis, W.T. Thompson, Coupled thermochemical, isotopic evolution and heat transfer simulations in highly irradiated UO₂ nuclear fuel, *J. Nucl. Mater.* 441 (2013) 240–251. doi:10.1016/j.jnucmat.2013.05.060.
- [14] K.T. Clarno, B. Philip, W.K. Cochran, R.S. Sampath, S. Allu, P. Barai, S. Simunovic, M.A. Berrill, L.J. Ott, S. Pannala, G.A. Dilts, B. Mihaila, G. Yesilyurt, J.H. Lee, J.E. Banfield, The AMP (Advanced MultiPhysics) Nuclear Fuel Performance code, *Nucl. Eng. Des.* 252 (2012) 108–120. doi:10.1016/j.nucengdes.2012.07.018.
- [15] H.S. Aybar, P. Ortego, A review of nuclear fuel performance codes, *Prog. Nucl. Energy.* 46 (2005) 127–141. doi:10.1016/j.pnucene.2005.01.004.
- [16] J.M. Vidal, J.P. Grouiller, A. Launay, Y. Berthion, A. Marc, H. Toubon, CESAR: A Code for Nuclear Fuel and Waste Characterisation, in: 2006.
- [17] B. Sundman, B. Jansson, J.-O. Andersson, The Thermo-Calc databank system, *Calphad.* 9 (1985) 153–190. doi:10.1016/0364-5916(85)90021-5.

- [18] H. Kleykamp, The Chemical State of Fission Products in Oxide Fuels, *J. Nucl. Mater.* 131 (1985) 221–246.
- [19] G. Ducros, Y. Pontillon, P.P. Malgouyres, Synthesis of the VERCORS experimental programme: Separate-effect experiments on Fission Product release, in support of the PHEBUS-FP programme, *Ann. Nucl. Energy.* 61 (2013) 75–87. doi:10.1016/j.anucene.2013.02.033.
- [20] A. Gallais-During, S. Bernard, B. Gleizes, Y. Pontillon, J. Bonnin, P.-P. Malgouyres, S. Morin, E. Hanus, G. Ducros, Overview of the VERDON-ISTP Program and main insights from the VERDON-2 air ingress test, *Ann. Nucl. Energy.* 101 (2017) 109–117. doi:10.1016/j.anucene.2016.09.045.
- [21] A. Gallais-During, J. Bonnin, P.-P. Malgouyres, S. Morin, S. Bernard, B. Gleizes, Y. Pontillon, E. Hanus, G. Ducros, Performance and first results of fission product release and transport provided by the VERDON facility, *Nucl. Eng. Des.* 277 (2014) 117–123. doi:10.1016/j.nucengdes.2014.05.045.
- [22] G. Ducros, Y. Pontillon, P.P. Malgouyres, Synthesis of the VERCORS experimental programme: Separate-effect experiments on Fission Product release, in support of the PHEBUS-FP programme, *Ann. Nucl. Energy.* 61 (2013) 75–87. doi:10.1016/j.anucene.2013.02.033.
- [23] Y. Pontillon, G. Ducros, Behaviour of fission products under severe PWR accident conditions. The VERCORS experimental programme—Part 3: Release of low-volatile fission products and actinides, *Nucl. Eng. Des.* 240 (2010) 1867–1881. doi:10.1016/j.nucengdes.2009.06.025.
- [24] J.-P. Hiernaut, T. Wiss, J.-Y. Colle, H. Thiele, C.T. Walker, W. Goll, R.J.M. Konings, Fission product release and microstructure changes during laboratory annealing of a very high burn-up fuel specimen, *J. Nucl. Mater.* 377 (2008) 313–324. doi:10.1016/j.jnucmat.2008.03.006.
- [25] C. Riglet-Martial, J. Sercombe, Y. Pontillon, Speciation and release kinetics of the Fission Products Mo, Cs, Ba and I from nuclear fuels in Severe Accidents conditions, in: *Transient Fuel Behav.*, Prague, Czech Republic, 2018.
- [26] T.-M.-D. Do, S. Sujatanond, Y. Tachibana, T. Ogawa, Vaporization and deposition of cesium dimolybdate, *Cs₂Mo₂O₇*, *J. Nucl. Sci. Technol.* 54 (2017) 330–336. doi:10.1080/00223131.2016.1273146.